Supporting Information

Construction of a thiourea-functionalized metal-organic macrocycle for the reductive amination of furfural under mild conditions.

Contents

1. Experimental Section.

Materials and methods:

The ligand BPTB was synthesized following the literature methods (Figure S2). All the chemicals and solvents were of reagent grade quality obtained from commercial sources and used without further purification.

Nuclear magnetic resonance:

^{1}H NMR spectra were recorded on Bruker spectrometers (400 MHz and 500 MHz), with chemical shifts referenced to the internal standard tetramethylsilane (TMS) at δ 0.0 ppm. ^{1}H DOSY spectra were measured on a Bruker 600MHz spectrometer.

Liquid chromatograph mass spectra:

ESI mass spectra were acquired on an Agilent G6224A HPLC-ESI-TOF/MS spectrometer, with acetonitrile/methanol as the mobile phase.

Liquid UV-Vis spectra:

Ultraviolet−Visible spectroscopy spectra were measured on a Shimadzu UV 2600 UV−Vis spectrophotometer.

Electrochemical experiments:

Cyclic voltammetry (CV) and square wave voltammetry (SWV) were performed on a CHI 670E electrochemical workstation using a three-electrode system: an Ag/AgCl reference electrode, a 0.5 mm diameter platinum wire counter electrode, and a glassy carbon working electrode. All measurements were conducted after purging the solutions with argon to remove oxygen interference.

High-performance liquid chromatography:

HPLC was performed on a SHIMADZU LC-2030 Plus system equipped with a ZORBAX SB-C18 column (250 ×4.6 mm I.D, s-5 μM) using methanol/water as mobile phase, to determine catalytic reaction yields.

Fluorescence spectra.

Fluorescence emission spectra of the solutions spectra were measured on an Edinburgh FLS1000 fluorescence spectrophotometer.

Single-Crystal X-ray diffraction

X-ray diffraction data were collected on a Bruker D8 Venture Photon II diffractometer with graphite monochromated Mo Kα radiation (λ = 0.71073 Å) or CuKα (λ=1.54178 Å). An empirical absorption correction using SADABS was applied for all data. The structures were solved by the dual methods using the SHELXS program.

All non-hydrogen atoms underwent anisotropic refinement by full matrix least-squares on F2 by the use of the program SHELXL[2], and hydrogen atoms were included in idealized positions with thermal parameters equivalent to 1.2 times those of the atoms to which they were attached. Some remaining Q peaks could not be successfully resolved despite numerous attempts at modeling, and consequently the SQUEEZE function of PLATON was used to account for these highly disordered solvents.[3]The atoms with huge ellipsoids in the crystals have been modelled as disordered over several sites. SIMU, DELU, ISOR, and runRIGU restraints have been applied to the non-hydrogen atoms with minor disorders. DFIX, SADI, DANG restraints are added to fix bond lengths. All non-hydrogen atoms underwent anisotropic refinement. Hydrogen atom positions were calculated geometrically**.**

Synthesis of Ligand

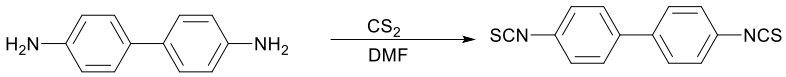

Figure S1 Synthesis of 4,4'-diisothiocyanato-1,1'-biphenyl

Synthesis of compound 4,4'-diisothiocyanato-1,1'-biphenyl: 4,4'-diaminobiphenyl (8mmol, 1.5g) was dissolved in 10 mL DMF, followed by the addition of 9 mL carbon disulfide and 2.25 mL triethylamine. After stirring at room temperature for 2 hours, 4.2 g O(7Azabenzotriazol1yl)N,N,N',N'-tetramethyluronium hexafluophosphate (HBTU) was added, and the mixture was kept stirring for an additional 15 minutes. The solvent was removed under reduced pressure by rotary evaporation, and the crude product was purified by silica gel column chromatography eluting with petroleum ether. The eluent was concentrated under reduced pressure to afford a white solid product, with an approximate yield of 70%.**^{1}H NMR**: (**400 MHz, DMSO**-d_6) δ 7.80 (d, J = 8.6 Hz, 44H), 7.55 (d, J = 8.8 Hz, 4H).

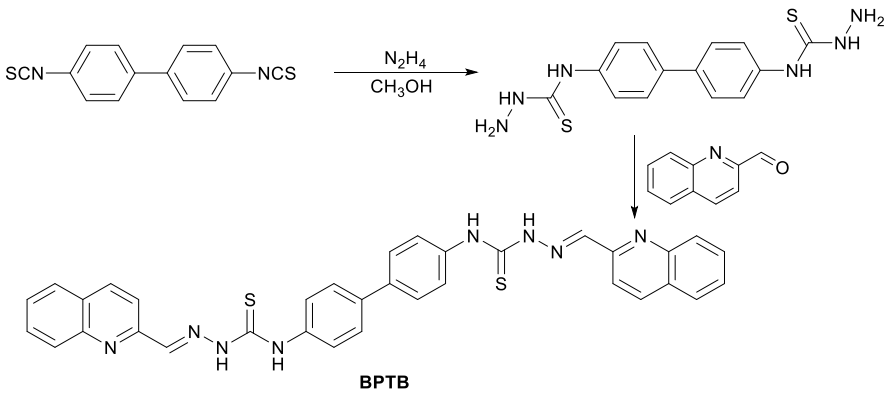

Figure S2 Synthesis of Ligand BPTB

Synthesis of Ligand BPTB[4]: 4,4'-diisothiocyanatobiphenyl (1.6mmol, 0.53g) was placed in a 100 mL round-bottom flask, and 30 mL anhydrous methanol was added as the solvent. Subsequently, 1.25 mL 80% hydrazine hydrate solution was added, and the mixture was stirred at 80 °C for 12 hours. The resulting product was filtered, washed with anhydrous methanol, and dried in vacuo to afford the precursor. The precursor required no further purification after drying. The precursor (0.62g) was placed in a 100 mL round-bottom flask, and 30 mL anhydrous methanol was added as the solvent. Then, 2-quinolinecarboxaldehyde (0.60 g) and glacial acetic acid (0.2 mL) were added, and the mixture was reacted at 80 °C for 24 hours. The resulting yellow solid was filtered, washed, and dried to afford ligand BPTB. **^{1}H NMR (400 MHz, DMSO-d$_6$)** δ 12.27 (s, 1H), 10.46 (s, 1H), 8.65 (d, *J* = 8.8 Hz, 1H), 8.43 (d, *J* = 8.8 Hz, 1H), 8.37 (s, 1H), 8.03 (dd, *J* = 13.5, 8.3 Hz, 2H), 7.83 – 7.58 (m, 6H).

Synthesis of macrocycle H$_1$: Ligand BPTB (0.1 mmol, 61 mg) and nickel (II) trifluoromethanesulfonate (0.1 mmol, 35 mg) were added to a 50 mL flask, followed by the addition of 20 mL acetonitrile. The mixture was purged with argon and subjected to vacuum cycles: the acetonitrile was first frozen with liquid nitrogen, followed by three vacuum–argon cycles. The mixture was heated at 70 °C for 24 h, during which the reaction solution gradually changed from pale yellow to deep red. After filtration through a membrane filter, the reaction solution was subjected to vapor diffusion using diethyl ether as the antisolvent, affording clear yellow needle-shaped crystals (yield: 65%).**^{1}H NMR (500 MHz, DMSO-d$_6$)** δ 12.36 (s, 1H), 10.57 – 10.48 (m, 1H), 8.70 (dd, *J* = 16.3, 8.7 Hz, 1H), 8.50 (d, *J* = 9.0 Hz, 1H), 8.42 – 8.35 (m, 1H), 8.05 (t, *J* = 8.4 Hz, 2H), 7.87 – 7.64 (m, 6H). **^{13}C NMR (126 MHz, DMSO-d$_6$)** δ 176.95, 153.11, 138.66, 137.25, 131.71, 128.72, 128.44, 128.39, 127.14, 127.03, 126.83, 126.70, 124.99, 122.43, 119.86, 119.23.

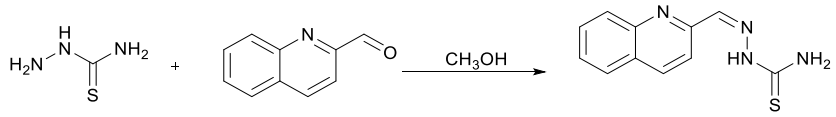

Figure S3 Synthesis of Mononuclear Complex Ligand

Synthesis of 2-(quinolin-2-ylmethylene) hydrazine-1-carbothioamide: thiosemicarbazide (4mmol, 0.91g) was placed in a 100 mL round-bottom flask, and 30 mL anhydrous methanol was added. Then, 2-quinolinecarboxaldehyde (0.62g) and glacial acetic (0.2 mL) acid were added, and the mixture was heated at 80 °C for 24 hours. The resulting

white solid was filtered, washed, and dried to afford the ligand.

^{1}H NMR (500 MHz, DMSO-d$_6$) δ 11.82 (s, 1H), 8.47 (d, *J* = 8.7 Hz, 2H), 8.39 – 8.33 (m, 2H), 8.23 (s, 1H), 8.00 (dd, *J* = 14.1, 9.1 Hz, 2H), 7.77 (t, *J* = 6.9 Hz, 1H), 7.62 (t, *J* = 7.5 Hz, 1H).

Synthesis of compound M$_1$: 2-(quinolin-2-ylmethylene) hydrazine-1-carbothioamide (0.1 mmol, 23 mg) and nickel (II) trifluoromethanesulfonate (0.1 mmol, 35 mg) were added to a 50 mL flask, followed by the addition of 20 mL acetonitrile. After vacuum degassing, the mixture was heated at 70 °C for 24 h, during which a clear yellow solution was obtained. Similarly, yellow block crystals were obtained by vapor diffusion (yield: 40%). **^{1}H NMR (500 MHz, DMSO-d$_6$)** δ 11.81 (s, 1H), 8.45 (t, J = 7.0 Hz, 2H), 8.37 (d, J = 8.7 Hz, 2H), 8.23 (s, 1H), 8.04 – 7.92 (m, 3H), 7.77 (d, J = 8.2 Hz, 1H), 7.62 (t, J = 7.8 Hz, 1H).

General procedure for reductive amination reactions

All catalytic reactions were conducted under isothermal conditions at room temperature. Furfural (50 μmol), aniline (50 μmol), and 0.5 μmol **H$_1$** were mixed in 5 mL acetonitrile solution, the mixture was purged with argon for 30 minutes to remove oxygen. Subsequently, 60 μmol sodium cyanoborohydride was added, and the reaction was allowed to proceed for 6 h. The yields of the products were determined by HPLC analysis performed on SHIMADZU LC or ^{1}H NMR using 1,3,5-trimethoxybenzene as internal standard.

The equations and the derivation

Michaelis-Menten Equation. [5] Michaelis-Menten equation was used to verify the mimic enzyme catalytic system.

$$V = V_{Max}\frac{[S]}{K_m + [S]}$$

Of which, V, the initial reaction rate of the enzymatic reactions; V_{max}, the maximum reaction rate of the enzymatic reactions; K_m, the Michaelis-Menten constant; [S], the concentration of the substrates. The equation could also transform into other form, like double-reciprocal plot showing below:

$$\frac{1}{V} = \frac{K_m}{V_{max}}\frac{1}{[S]} + \frac{1}{V_{max}}$$

Randles-Sevcik Equation. Randles-Sevcik equation was used to calculate the apparent diffusion coefficient of the **H1**

$$i_p = 0.4463nFAC\left(\frac{nFvD}{RT}\right)^{\frac{1}{2}}$$

Of which, i_p, the current maximum in amps; n, the number of electrons transferred in the redox event; A, electrode area in cm^2; F, faraday constant in C mol^{-1}; D, diffusion coefficient in cm^2/s; C, concentration in mol/cm^3; ν, scan rate in V/s; R, gas constant in J K^{-1} mol^{-1}; T, temperature in K.

For the nonlinear fitting of the host-guest complex system[5]

For a 1:1 encapsulation process:

$$H + G \rightleftharpoons HG$$

Here, *H* represents the host in the system, *G* represents the guest, and *HG* represents the host–guest inclusion complex formed in the system.

$$[HG] = K_a[H][G] = K_a([H]_0 - [HG])([G]_0 - [HG])$$

Here, K_a denotes the association constant for the formation of the host–guest inclusion complex in the system, *[H]* denotes the concentration of the host, *[G]* denotes the concentration of the guest, and *[HG]* denotes the concentration of the host–guest inclusion complex formed.

Rearranging the equation gives:

$$[HG]^2 - \left([H]_0 + [G]_0 + \frac{1}{K_a}\right)[HG] + [H]_0[G]_0 = 0$$

The solution to this quadratic equation is:

$$[HG] = \frac{\left([H]_0 + [G]_0 + \frac{1}{K_a}\right) - \sqrt{\left([H]_0 + [G]_0 + \frac{1}{K_a}\right)^2 - 4[H]_0[G]_0}}{2}$$

For the UV–Vis absorption or fluorescence spectra obtained from titration of the host–guest complex in the system, a signal exists at any given point such that:

$$y = a[HG] + b[H] + c[G] = (a - b - c)[HG] + b[H]_0 + c[G]_0$$

Here, **a**, **b**, and **c** are specific constants.

$$y = (a - b - c)\frac{\left([H]_0 + [G]_0 + \frac{1}{K_a}\right) - \sqrt{\left([H]_0 + [G]_0 + \frac{1}{K_a}\right)^2 - 4[H]_0[G]_0}}{2} + b[H]_0 + c[G]_0$$

The relationship between the titration signal **y** and the initial concentration of the guest added to the system, **[G]$_0$**, can be fitted using this equation.

In general, since the guest usually shows no response at the corresponding signal position (no fluorescence response or no absorption in the visible region), the equation can be simplified to:

$$y = a[HG] + b[H] = (a - b)[HG] + b[H]_0$$

$$y = (a - b)\frac{\left([H]_0 + [G]_0 + \frac{1}{K_a}\right) - \sqrt{\left([H]_0 + [G]_0 + \frac{1}{K_a}\right)^2 - 4[H]_0[G]_0}}{2} + b[H]_0$$

Let $k = (a - b),\ y_0 = b[H]_0$

$$y = k\frac{\left([H]_0 + [G]_0 + \frac{1}{K_a}\right) - \sqrt{\left([H]_0 + [G]_0 + \frac{1}{K_a}\right)^2 - 4[H]_0[G]_0}}{2} + y_0$$

This equation is the nonlinear fitting relationship between the titration signal **y** and the initial concentration of the guest added to the system, **[G]$_0$**, for the titration of a 1:1 host–guest inclusion complex.

Stokes-Einstein Equation[6,7]

The Stokes–Einstein (SE) equation is a fundamental hydrodynamic relationship used to calculate the hydrodynamic radius of a particle in a solution.

The standard form of the Stokes–Einstein equation is expressed as follows:

$$D = \frac{k_B T}{6\pi\eta R_h}$$

Rearranged to solve for the hydrodynamic radius (R_h):

$$R_h = \frac{k_B T}{6\pi\eta D}$$

Of which, D, the translational diffusion coefficient of the particle in solution in cm^2/s; k_B, the Boltzmann constant in $J \cdot K^{-1}$; T, the absolute temperature of the solution in K; η, the dynamic viscosity of the solvent in Pa·s; R_h, the hydrodynamic radius of the particle in m.

The Stokes–Einstein equation was derived by assuming that a spherical particle of colloidal dimension (much higher than that of the solvent) moves with uniform velocity in a fluid continuum. The modified Stokes–Einstein equation that takes into account both the relative solute/solvent size and the shape of the molecules is:

$$D_t = \frac{kT}{c(r_{solv}, r_H) f_s(a,b) \pi\eta r_H}$$

The c factor[8] is:

$$c = \frac{6}{1 + 0.695\left(\frac{r_{solv}}{r_H}\right)^{2.234}}$$

For an oblate ellipsoid, another correction factor (f_s)[9]:

$$f_S = \frac{\sqrt{\left(\frac{b}{a}\right)^2 - 1}}{\left(\frac{b}{a}\right)^{\frac{2}{3}} \arctan\left(\sqrt{\left(\frac{b}{a}\right)^2 - 1}\right)}$$

2. Single Crystal X-ray Crystallography

Table S1. Crystal data and structure refinement of H_0.

Compound	BPTB-Ni(H_0)
Empirical formula	$C_{324}H_{426}F_{36}N_{48}Ni_6O_{63}S_{24}$
Formula weight	7806.80
Temperature/K	200.0
Crystal system	monoclinic
Space group	$P2_1/n$ (14)
a/Å	18.981(9)
b/Å	37.381(11)
c/Å	58.275(12)
α/ °	90
β/ °	95.90(2)
γ/ °	90
Volume/Å^3	41129.2(15)
Z	4
ρ_{calc}g/cm^3	1.261
μ/mm^{-1}	2.165
F (000)	16344
Crystal size/mm^3	0.16×0.17×0.18
Radiation	CuKα (λ=1.54178 Å)
2θ range [°]	3.86 to 72.97 (1.30 Å)
Index ranges	−14 ≤ h ≤ 14 −28 ≤ k ≤ 28 −44 ≤ l ≤ 44
Reflections collected	136379
Independent reflections	19634 [R_{int} = 0.1404, R_{sigma} = 0.1132]
Data/restraints/parameters	19634 / 4625 / 2145
Goodness-of-fit on F^2	1.765
Final R indexes [$I>=2\sigma(I)$]	R_1 = 0.1428, wR_2 = 0.3574
Final R indexes [all data]	R_1 = 0.1872, wR_2 = 0.3784
Largest diff. peak/hole / e Å^{-3}	0.59/−0.39
CCDC number	2527682

Table S2. Crystal data and structure refinement of M_1.

Compound	M_1
Empirical formula	$C_{30}H_{35}F_6N_8NiO_{7.5}S_4$
Formula weight	928.68
Temperature [K]	173.00
Crystal system	monoclinic
Space group (number)	$P2/n$ (13)
a [Å]	18.1272(8)
b [Å]	11.2488(5)
c [Å]	21.1590(10)
α [°]	90
β [°]	108.756(2)
γ [°]	90
Volume [Å^3]	4085.4(3)
Z	4
ρ_{calc} [gcm^{-3}]	1.510
μ [mm^{-1}]	0.761
F(000)	1908
Crystal size [mm^3]	0.16×0.17×0.18
Radiation	MoK_α (λ=0.71073 Å)
2θ range [°]	4.45 to 58.06 (0.73 Å)
Index ranges	$-24 \le h \le 24$
	$-15 \le k \le 15$
	$-28 \le l \le 28$
Reflections collected	98568
Independent reflections	10883 [R_{int} = 0.0803 R_{sigma} = 0.0429]
Data / Restraints / Parameters	10883 / 59 / 537
Absorption correction T_{min}/T_{max}	0.6364 / 0.7458
(method)	(none)
Goodness-of-fit on F^2	1.037
Final R indexes	R_1 = 0.0438
[$I \ge 2\sigma(I)$]	wR_2 = 0.1038
Final R indexes	R_1 = 0.0656
[all data]	wR_2 = 0.1175
Largest peak/hole [eÅ^{-3}]	0.63/−0.62
CCDC number	2527681

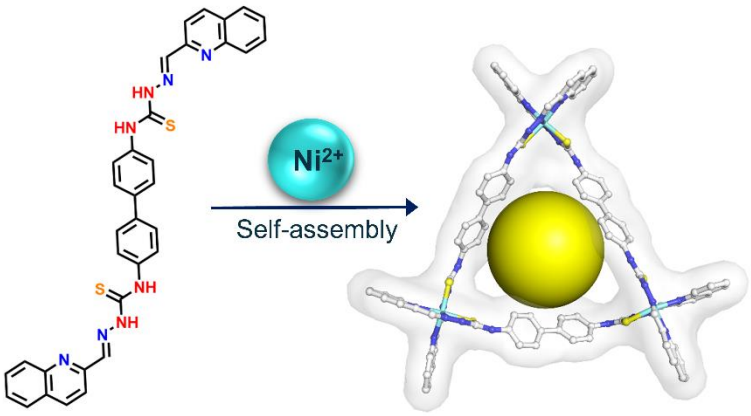

Figure S4. The self-assembly process of $\mathbf{H_1}$ and the inner cavity (yellow balls), where nickel, nitrogen, sulfur and carbon atoms are shown in pale blue, blue, pale yellow and grey respectively.

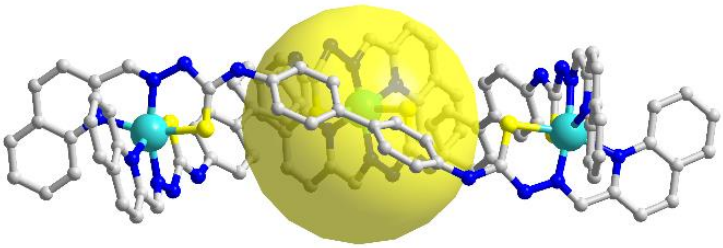

Figure S5. The cavity constructed by $\mathbf{H_1}$; its approximate radius is 5.3 Å.

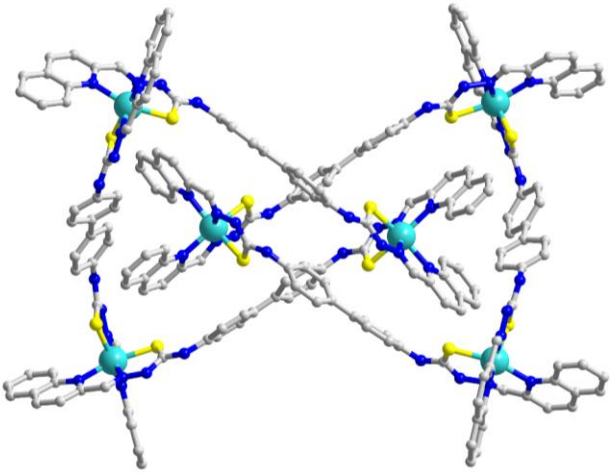

Figure S6. The crystal structure of $\mathbf{H_0}$. It features two interlocked $\mathbf{H_1}$ in its structure, where nickel, nitrogen, sulfur and carbon atoms are shown in pale blue, blue, pale yellow and grey respectively.

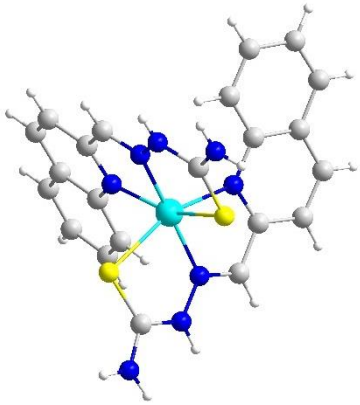

Figure S7. The crystal structure of the **M1**, where nickel, nitrogen, sulfur and carbon atoms are shown in pale blue, blue, pale yellow and grey respectively.

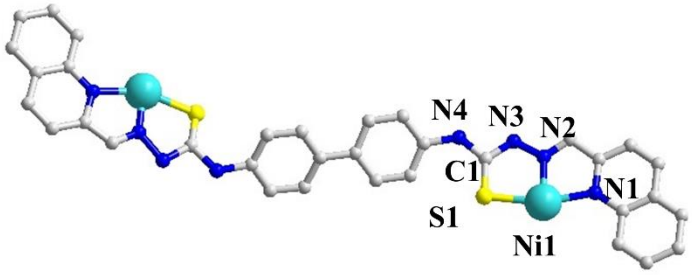

Figure S8. Molecular structure of **H1** within a unique asymmetric unit, showing the backbone of the ligand in the complex. Selected bond distances (Å): Ni1-N1 2.111(11), Ni1-N2 2.05(2), Ni1-S1 2.377(8), N2-N3 1.39(2), C1-S1 1.55(2), C1-N3 1.355(17) C1-N4 1.345(16).

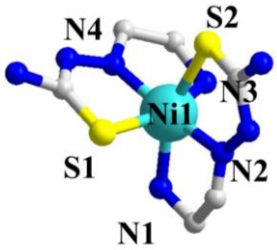

Figure S9. Coordination geometry of the Ni atom in **H1**. Selected angles (°): S1-Ni1-S2 95.5(2), N3-Ni1-S1-158.4(4), N3-N1-S2 91.4(4), N3-Ni1-N4-92.3(4), N1-Ni1-S1 88.1(3), N1-Ni1-S2 160.0(4), N4-N1-S1 78.3(7), N4-N1-S2 90.0(6), N4-N1-N3 81.3(8), N4-N1-N00S 110.0(6), N2-N1-S1 90.9(6), N2-N1-S2 82.2(7), N2-N1-N3 110.4(7), N2-N1-N00S 78.1(7), N2-N1-N4 166.1(8)

3. Experimental Details.

UV-Vis spectra

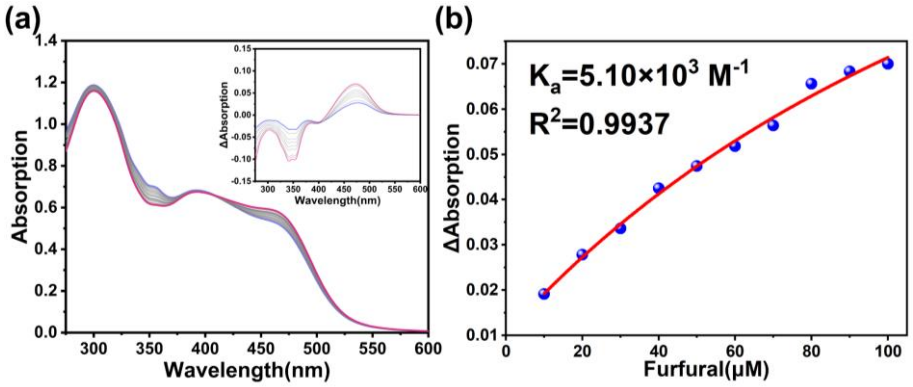

Figure S10. (a) UV-Vis spectra and difference spectra of the **H1** (0.01 mM) upon the addition of furfural in an acetonitrile solution. (b) The nonlinear fitting of the titration curve (recorded absorption at 475 nm), showing a 1:1 host-guest binding stoichiometry between **H1** and furfural with an association constant calculated as 5.10 × 10^3 M^{-1}.

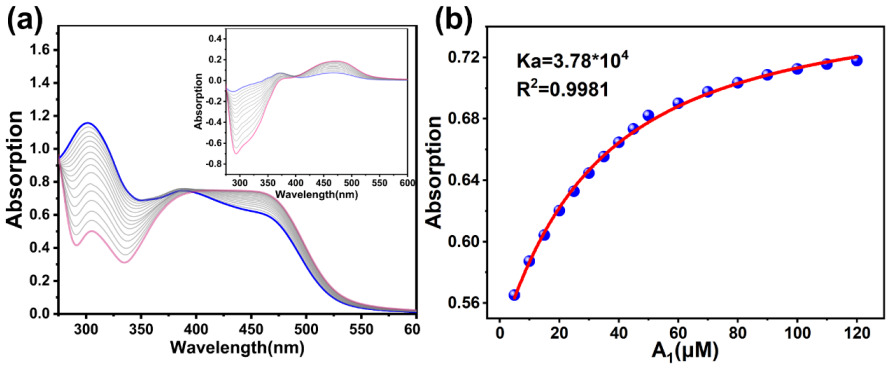

Figure S11. (a) UV-Vis spectra of the **H1** (0.01 mM) upon the addition of **A1** in an acetonitrile solution. (b) The nonlinear fitting of the titration curve (recorded absorption at 475 nm), showing a 1:1 host-guest binding stoichiometry between **H1** and **A1** with an associated constant calculated as 3.68 × 10^4 M^{-1}.

Nuclear magnetic resonance

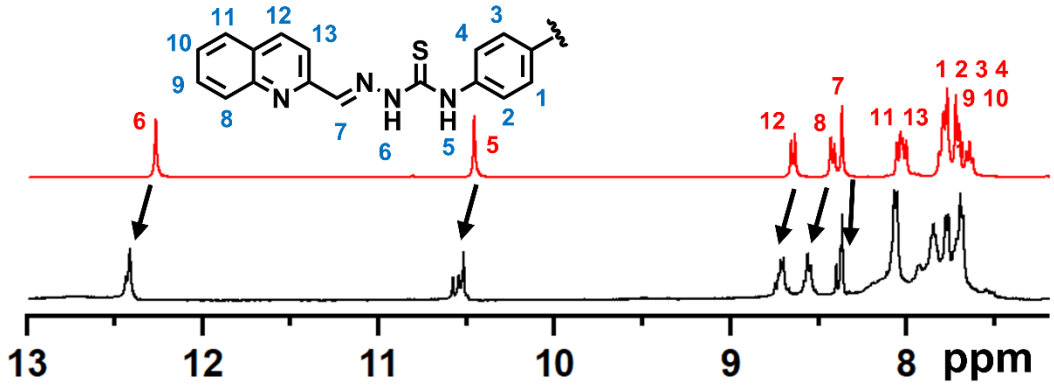

Figure S12. ^{1}H NMR spectrum of **H$_1$** (black line) and **BPTB** (red line)

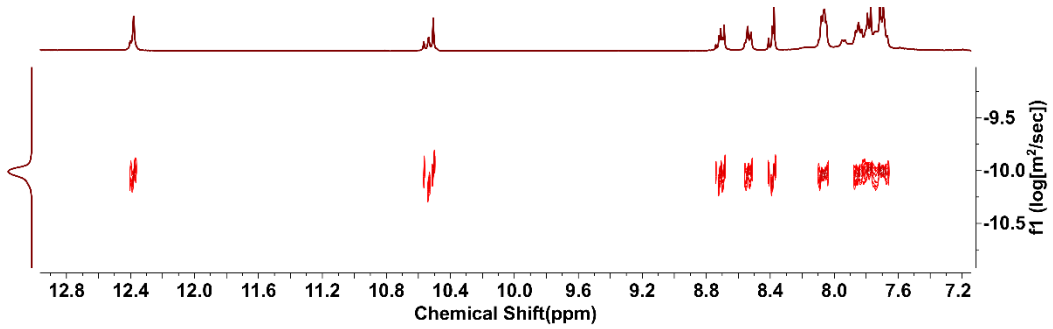

Figure S13. The ^{1}H DOSY spectrum of **H$_1$** (600 MHz, DMSO-d$_6$, 298K). The diffusion coefficient is 9.93 × 10^{-11} $m^2 \cdot s^{-1}$ in this solution.

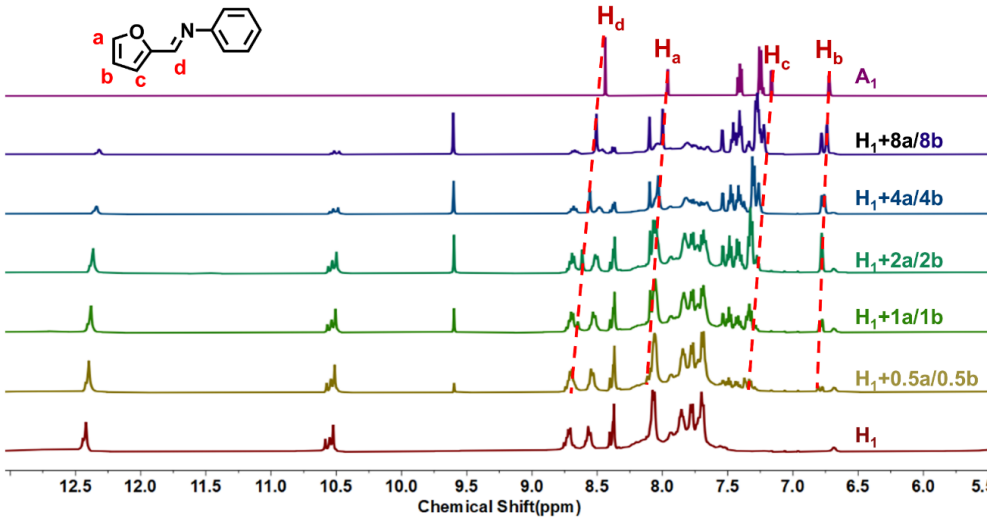

Figure S14. ^{1}H-NMR titration spectra of the macrocycle **H$_1$** upon addition of a mixed solution of furfural and aniline (the mixture was reacted for 1 h prior to NMR measurement) (500 MHz, DMSO-d$_6$, 298K).

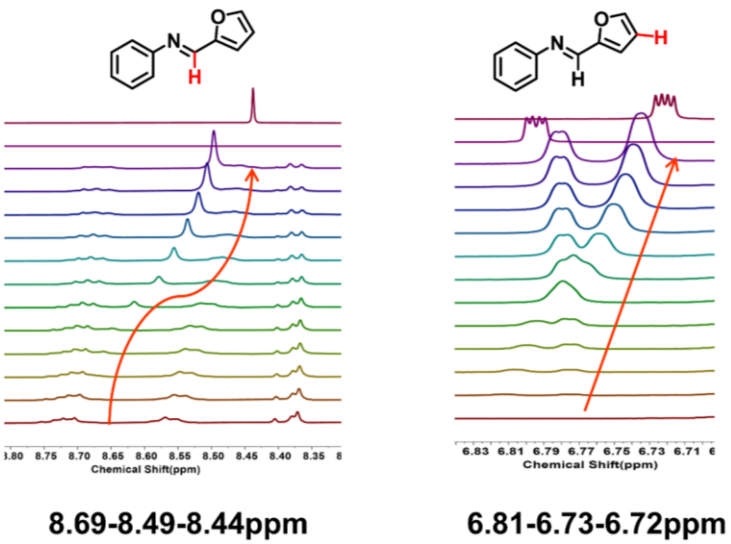

Figure S15. Enlarged view of the ^{1}H NMR titration showing two prominent chemical shifts of the imine substrate at 8.44–8.69 ppm and 6.72–6.81 ppm. (500 MHz, DMSO-d_6, 298K).

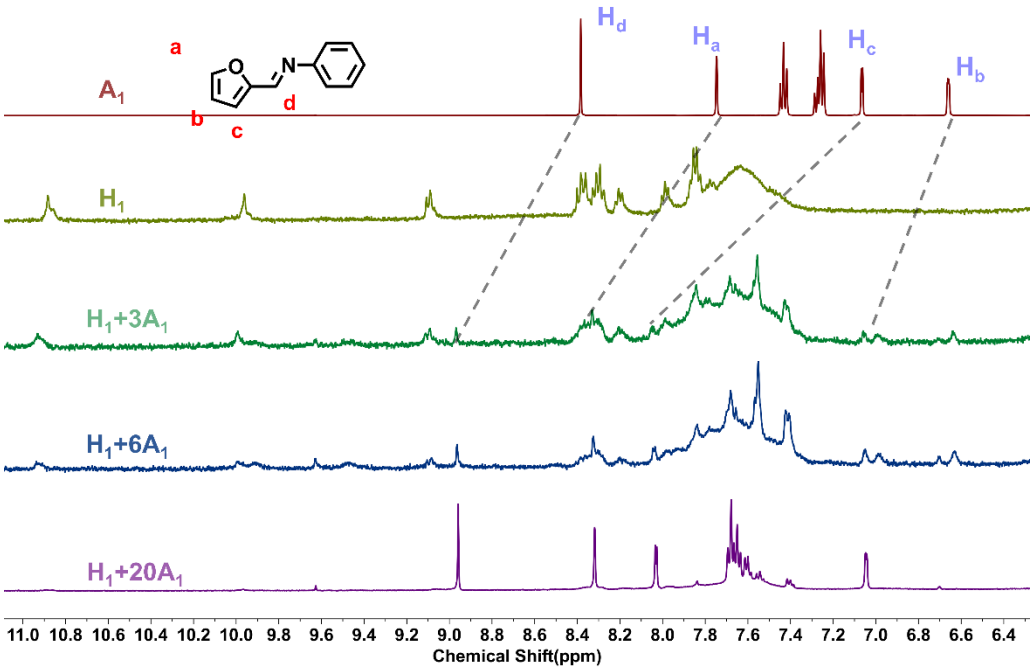

Figure S16. ^{1}H-NMR titration spectra of the macrocycle **H1** upon addition of A_1 (400MHz, CD_3CN, 298K)

Calculation of hydrodynamic radius

The hydrodynamic radius was calculated according to the standard Stokes–Einstein equation for spherical particles without correction:

$$R_h = \frac{k_B T}{6\pi\eta D}$$

where k_B is the Boltzmann constant, T = 298 K, η is the viscosity of DMSO at 25 °C, and D is the measured diffusion coefficient. Using D = 9.93 × 10^{-11} m^2/s and η = 1.996 × 10^{-3} Pa · s, the corresponding hydrodynamic radius was determined to 11.1 Å.

The macrocycle **H1** can be regarded as a triangular disk with a side length of 1.8 nm and a height of 0.4 nm. The modified Stokes–Einstein equation that takes into account both the relative solute/solvent size and the shape of the molecules is:

$$D_t = \frac{kT}{c(r_{solv}, r_H) f_s(a,b) \pi \eta r_H}$$

The shape factor fs was calculated using the following expression:

$$f_S = \frac{\sqrt{\left(\frac{b}{a}\right)^2 - 1}}{\left(\frac{b}{a}\right)^{\frac{2}{3}} \arctan\left(\sqrt{\left(\frac{b}{a}\right)^2 - 1}\right)}$$

where a=0.2 nm and b=0.67 nm (the radius of a circle with equivalent area to **H1**). Substituting these values yields a shape factor of fs ≈ 1.12.

The factor c is defined as:

$$\frac{6}{1 + 0.695\left(\frac{r_{solv}}{r_H}\right)^{2.234}}$$

where r_{solv} denotes the hydrodynamic radius of DMSO, taken as 2.63 Å from the literature[10]. By substituting the experimental diffusion coefficient Dt = 9.93 × 10^{-11} $m^2 \cdot s^{-1}$ and the geometric shape factor fs = 1.12 into the Stokes–Einstein equation, the hydrodynamic radius $\mathbf{r_H}$ was determined to be **10.2** Å.

ESI-MS spectrum

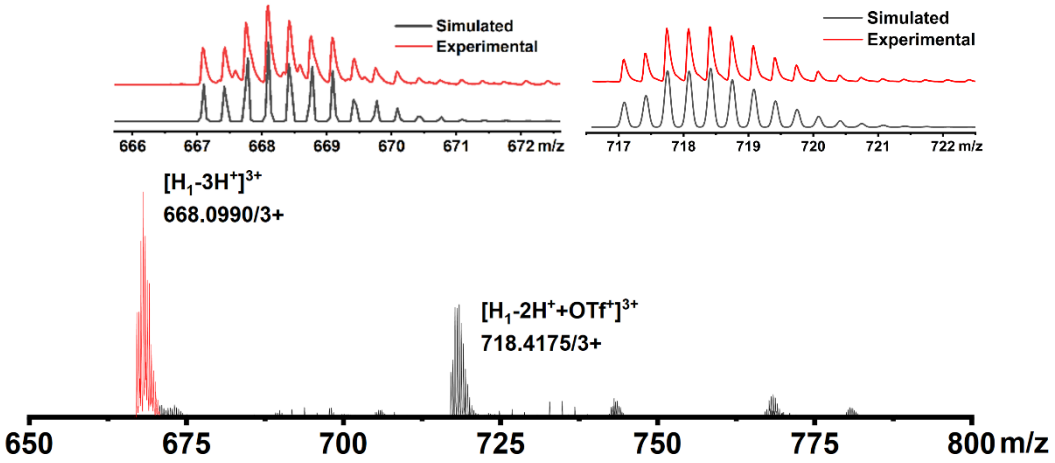

Peaks	Value of m/z	Species assigned
1	668.0990/3+	$[H_1\text{-}3H^+]^{3+}$
2	718.1475/3+	$[H_1\text{-}2H^+\text{+}OTf^-]^{3+}$

Figure S17. The ESI-MS spectrum of **H1** (0.10 mM) in CH_3CN solution. The inserts show the measured and simulated isotopic patterns at m/z = 668.0990 and 718.4175.

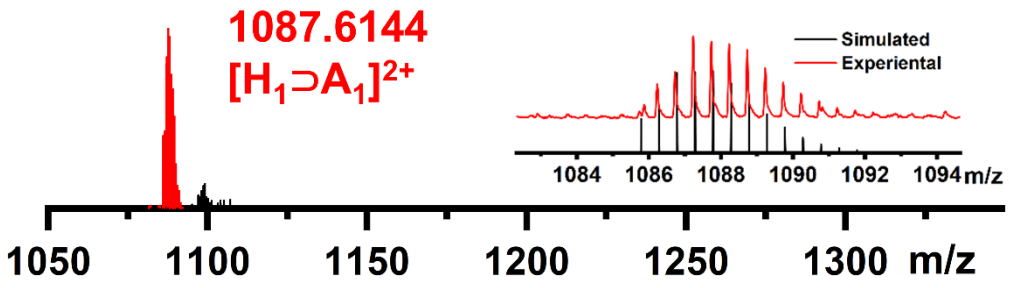

Figure S18. The ESI-MS spectrum of **H1** (0.10 mM), furfural (0.20 mM), aniline(0.20mM) in CH_3CN solution. The inserts show the measured and simulated isotopic patterns of the host-guest mixture at m/z = 1087.6144. This species is assigned to $[\mathbf{H_1}\text{-}4H^+\text{+}\mathbf{A_1}]^{4+}$.

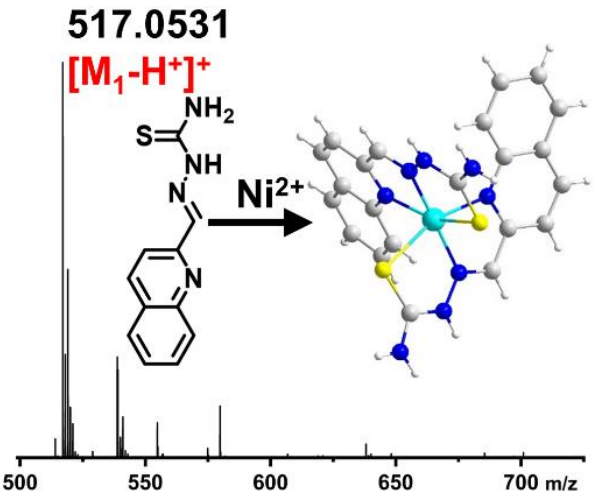

Figure S19. The ESI-MS spectrum of **M1** (0.10 mM) in CH_3CN solution. The inserts show the measured and simulated isotopic patterns at m/z = 517.0531. This species is assigned to $[\mathbf{M_1}\text{-}H^+]^+$.

Luminescence Spectra

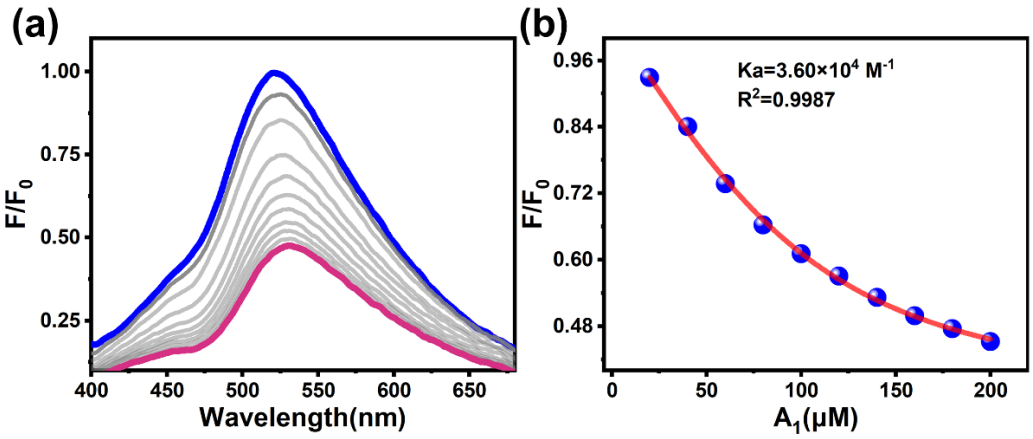

Figure S20 (a) The emission spectra of **H1** (0.10 mM) upon addition of **A1**. (b) The nonlinearity fitting of the titration curve showing a 1:1 host-guest behavior between **H1** and **A1** with a constant of 3.60×10^4 M^{-1}.

Electrochemical experiments.

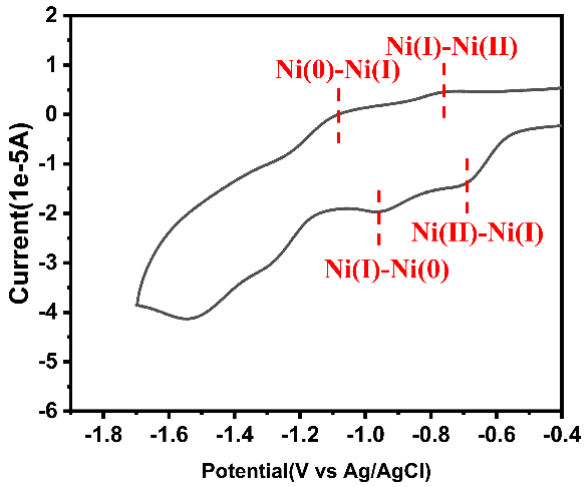

Figure S21. Cyclic voltammetry curves at different scan rates for **H₁** (0.10 mM) in DMSO solution containing 0.10 M TBAOTf.

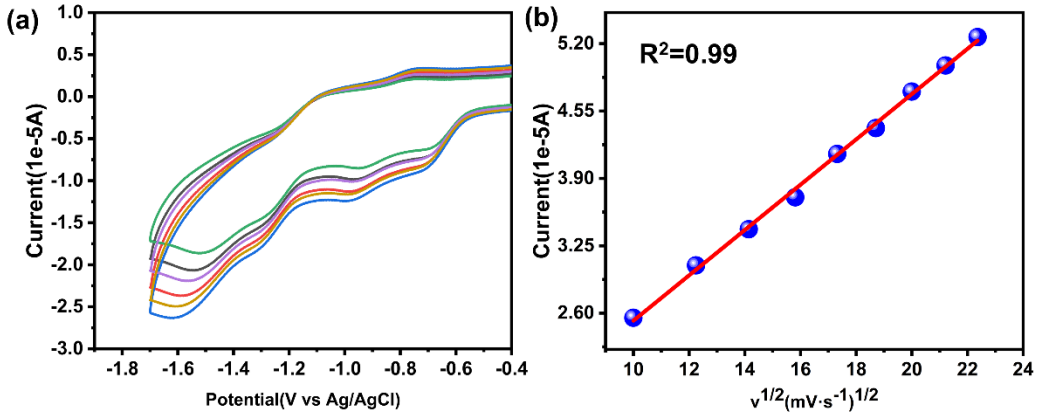

Figure S22. (a) The scan rate in cyclic voltammetry was linearly increased in a DMSO solution of 0.10 mM **H₁** at various rates. (b) Plotting peak current versus the square root of the scan rate revealed a linear relationship, which was consistent with the Randles-Sevcik equation and indicated diffusion-controlled electrochemical behaviour with a diffusion coefficient of 1.05×10^{-10} m^2 s^{-1}.

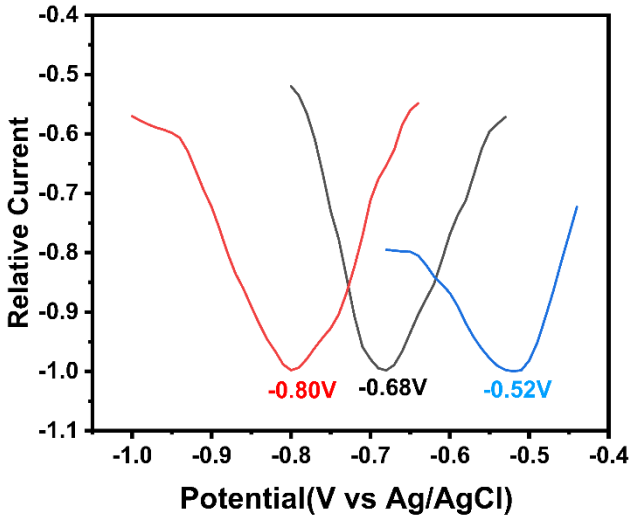

Figure S23. SWV spectra of the imine intermediate in acetonitrile solution upon addition of **H1** (0.10 mM). The reduction potential of the imine intermediate shifts from -0.80 V to -0.68 V upon addition of 0.5 equiv. of **H1**, and further to -0.52 V upon addition of another 0.5 equivalent.

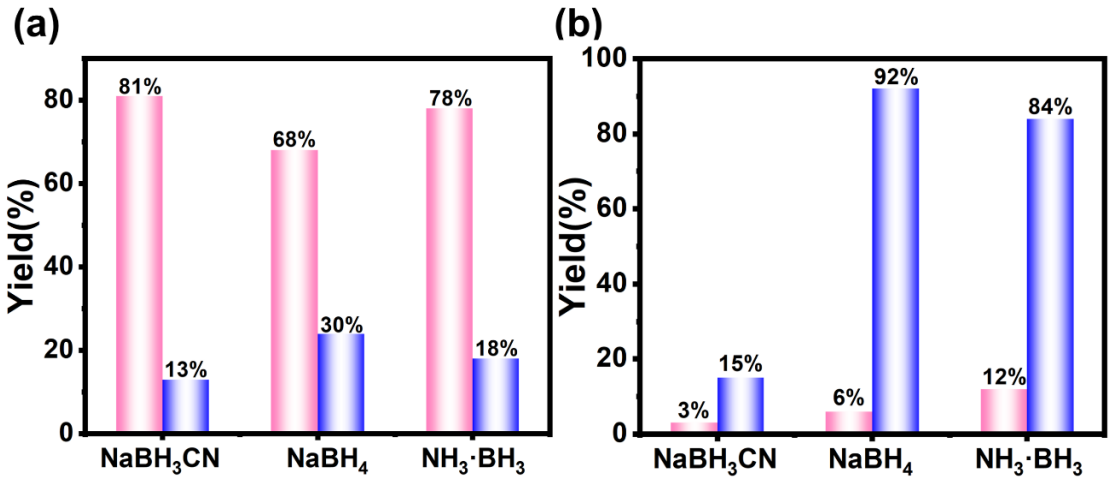

Figure S24. Yields of the product with different reducing agents after reaction at room temperature for 6 hours**.** (a): catalyzed by **H1** (b): without **H1** Pink bar: N-(furan-2-ylmethyl)aniline Blue bar: furfuryl alcohol

Table S3. Optimization of Reaction Conditions.

Entry	Variations from standard conditions	[a]Yield (%)
1	None	81
2	No **H_1**	15
3	L_1 instead of **H_1**	22
4	$Ni(OTf)_2$ instead of **H_1**	15
5[b]	**M_1** instead of **H_1**	45
6	$NaBH_4$ instead of $NaBH_3CN$	68
7	NH_3BH_3 instead of $NaBH_3CN$	78
8[c]	ATPNa	46

[a]Standard conditions: furfural (0.05 mmol), aniline (0.05 mmol), 1mol% **H_1** (0.5 μmol), $NaBH_3CN$ (0.06 mmol) and CH_3CN (5 mL). The mixture was reacted at room temperature in an argon atmosphere for 6h. [b]M_1: A mononuclear complex synthesized from thiosemicarbazide, 2-quinolinecarboxaldehyde, and $Ni(OTf)_2$. [c]1μmol ATPNa was added as an inhibitor for the catalytic reaction. Stir ATPNa with **H_1** for 30 minutes before adding substrates. The yields were determined by NMR using 1,3,5-trimethoxybenzene as internal standard.

Table S4: Substrate scope of Reductive Amination

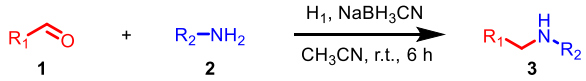

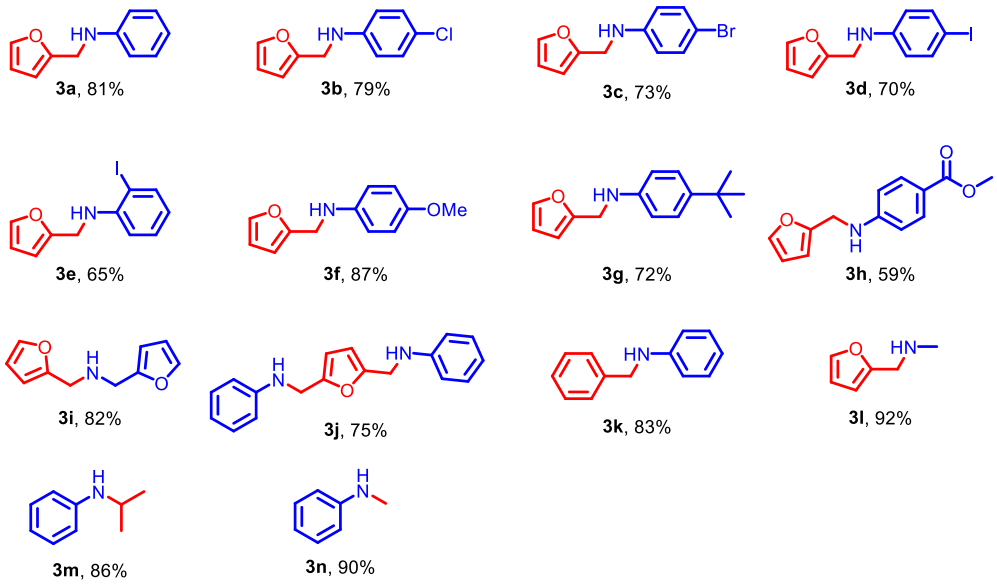

Standard conditions: furfural (0.05 mmol), aniline (0.05 mmol) and 1mol% **H1** (0.5 μmol) $NaBH_3CN$ (0.06 mmol) and CH_3CN (5 mL). The mixture was reacted at room temperature in an argon atmosphere for 6 h. The yields were determined by NMR using 1,3,5-trimethoxybenzene as internal standard.

Recycling experiments

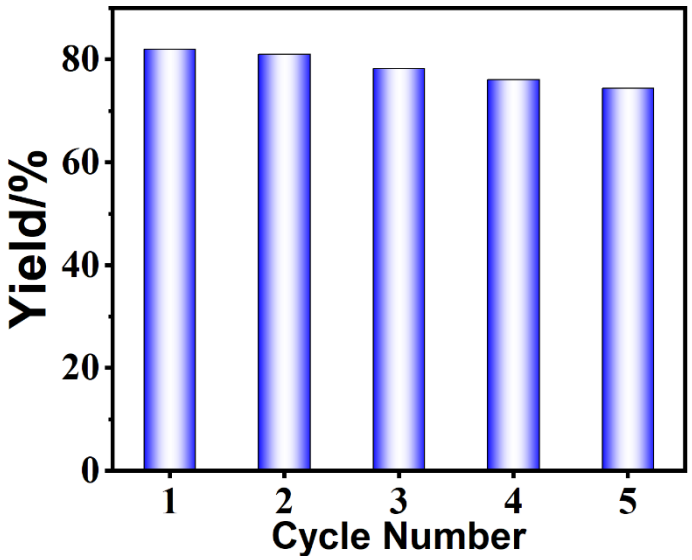

Figure **S25.** Conducting circular experiments and assessment of catalyst durability under standard conditions.

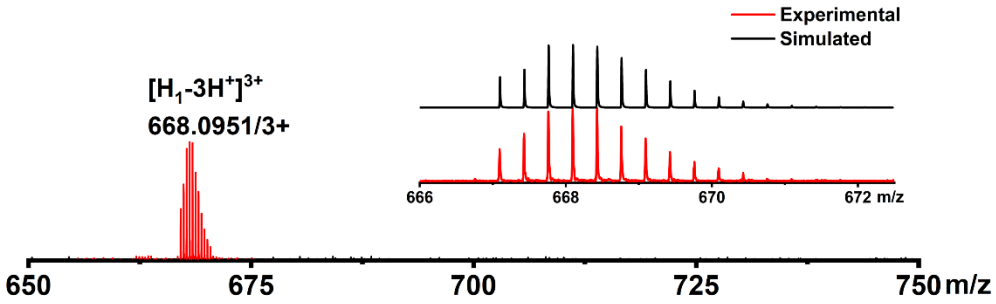

Figure **S26.** The ESI-MS spectrum of $\mathbf{H_1}$ after reaction under standard conditions.

Kinetics experiments

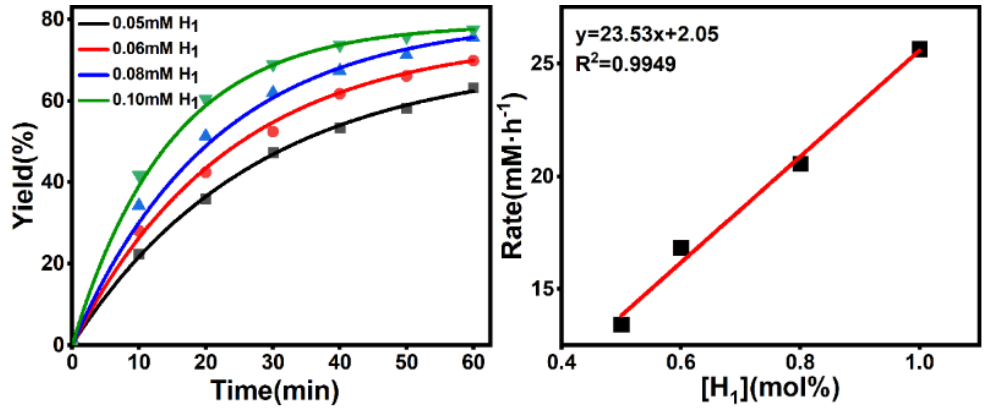

Figure S27. (a) Kinetics experiments of furfural and aniline condensation reaction at different **H1** concentrations. (b) Initial rate of reaction as a function of **H1** concentration.

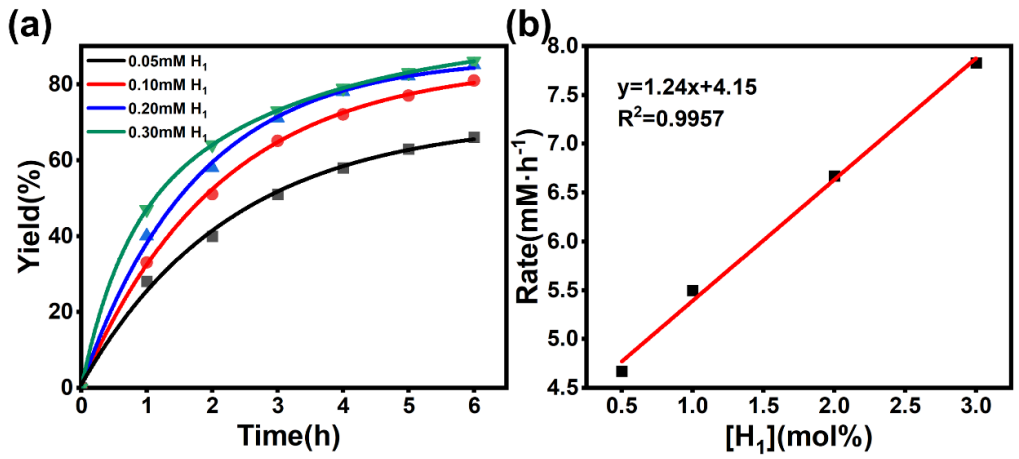

Figure S28. (a) Kinetics experiments of reductive animation at different **H1** concentrations. (b) Initial rate of reaction as a function of **H1** concentration

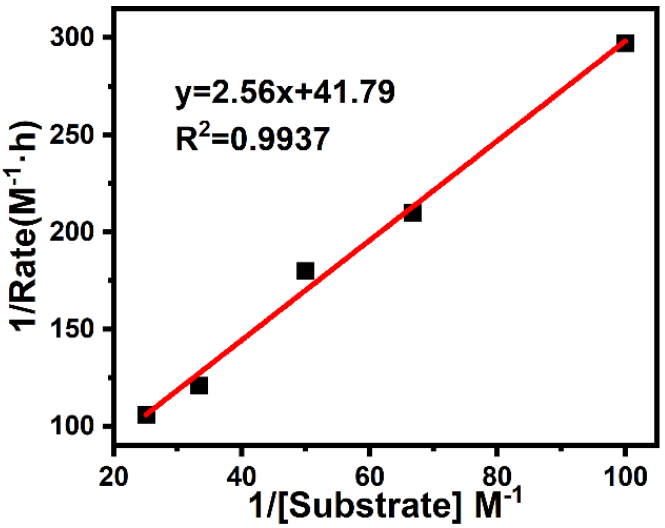

Figure S29. The Lineweaver–Burk double-reciprocal plot of initial reaction rate versus the concentration of the furfural-aniline mixture, indicating that the catalytic process follows a Michaelis–Menten kinetic mechanism.

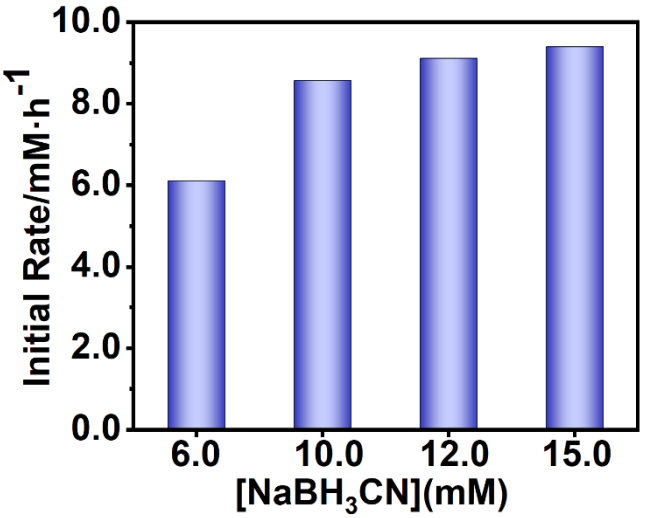

Figure S30. Initial rate of reductive animation at different $NaBH_3CN$ concentrations.

ATP competitive inhibition experiments

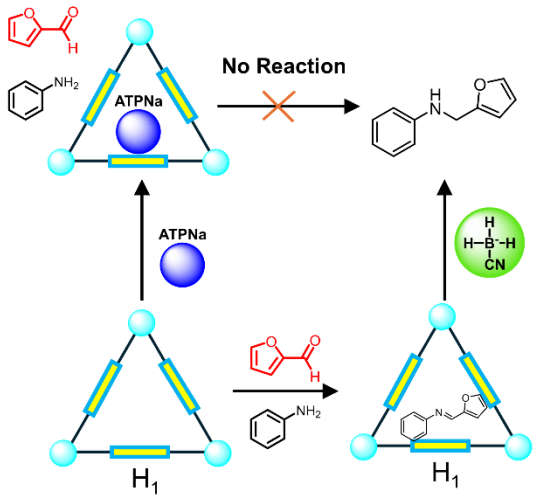

Figure S31. Schematic illustration of ATP competitive inhibition in the **H_1**-catalyzed system

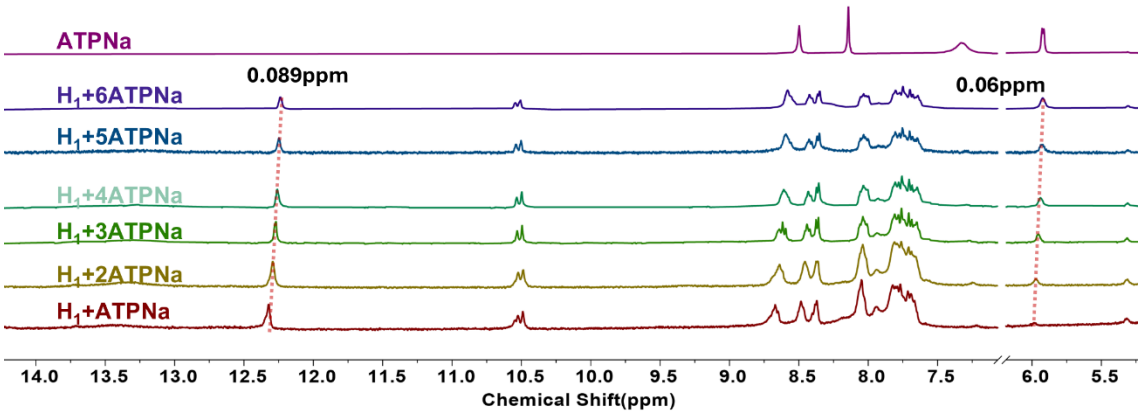

Figure S32. ¹H-NMR titration spectra of the macrocycle **H_1** upon addition of ATPNa (400MHz, DMSO-d_6, 298K)

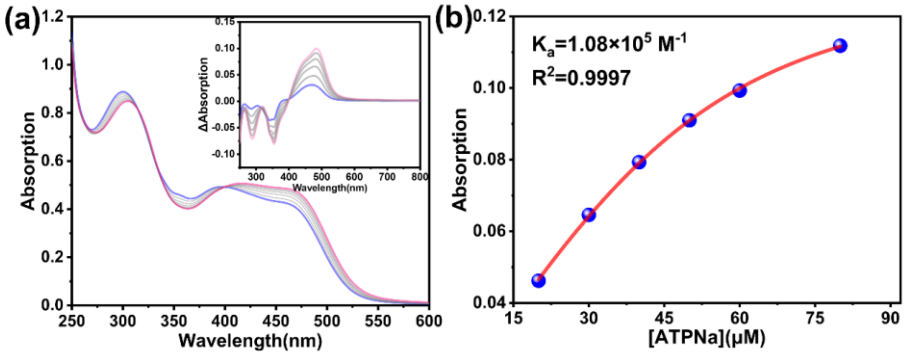

Figure S33. (a) UV-Vis spectra and difference spectra of the **H$_1$** (0.01 mM) upon the addition of ATPNa in an acetonitrile solution. (b) The nonlinear fitting of the titration curve (recorded absorption at 475 nm), showing a 1:1 host-guest behavior between **H$_1$** and ATPNa with an associated constant calculated as 1.08 × 10^5 M^{-1}.

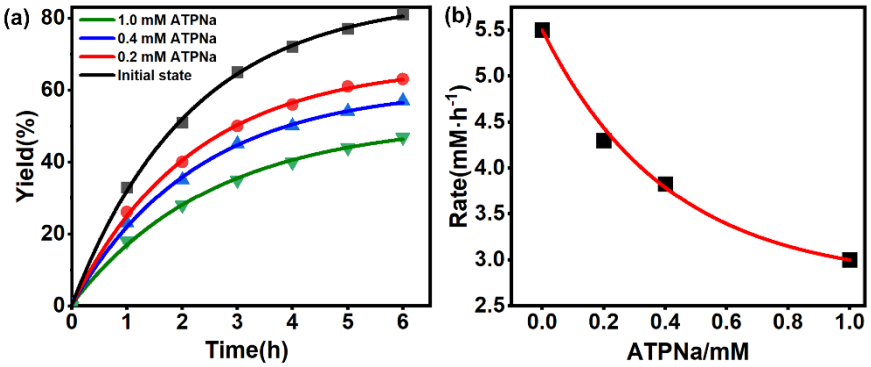

Figure S34. (a) Kinetic inhibition profiles upon titration of ATPNa into the **H$_1$** catalytic system. (b) Initial rate of reaction as a function of ATPNa concentration.

Table S5: **Comparison of Catalytic Performance of H_1 with Reported Works**

Number	Catalysts	Conditions	Yield	Reference
1	**$Ni_3L_3(H_1)$**	**$NaBH_3CN$**	**81%**	**this work**
2	Fe_4L_6	$NaBH_3CN$	65%[a]	Ref[11]
3		167030-40-2[b]	78%	Ref[12]
4	1343-93-7[c]	$NaBH_4$	86%	Ref[13]
5	1173000-70-8[d]	Phenylsilane	89%	Ref[14]
6	AuNPore	Dimethylphenylsilane	64%	Ref[15]
7	Pd@Fe_3O_4-NH_2/Starch	Hydrogen	85%	Ref[16]

a: Yield of furfuryl alcohol; b: Tin, dibutylchloro(hexamethyl phosphoric triamide-kO)hydro-, (TB-5-12)-(9Cl); c: 12-Tungstophosphoric acid; d: 1*H*-Imidazolium, 3-[6-(dibutylchlorostannyl)hexyl]-1-methyl-, iodide (1:1)

4. Characterization Data for All Compounds

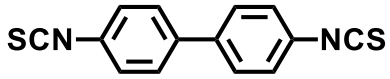

^{1}H NMR (400 MHz, DMSO-d$_6$) δ 7.80 (d, *J* = 8.6 Hz, 44H), 7.55 (d, *J* = 8.8 Hz, 4H).

BPTB

^{1}H NMR (400 MHz, DMSO-d$_6$) δ 12.27 (s, 1H), 10.46 (s, 1H), 8.65 (d, *J* = 8.8 Hz, 1H), 8.43 (d, *J* = 8.8 Hz, 1H), 8.37 (s, 1H), 8.03 (dd, *J* = 13.5, 8.3 Hz, 2H), 7.83 – 7.58 (m, 6H).

H$_1$

^{1}H NMR (500 MHz, DMSO-d$_6$) δ 12.36 (s, 1H), 10.57 – 10.48 (m, 1H), 8.70 (dd, *J* = 16.3, 8.7 Hz, 1H), 8.50 (d, *J* = 9.0 Hz, 1H), 8.42 – 8.35 (m, 1H), 8.05 (t, *J* = 8.4 Hz, 2H), 7.87 – 7.64 (m, 6H).

^{13}C NMR (126 MHz, DMSO-d$_6$) δ 176.95, 153.11, 138.66, 137.25, 131.71, 128.72, 128.44, 128.39, 127.14, 127.03, 126.83, 126.70, 124.99, 122.43, 119.86, 119.23**.**

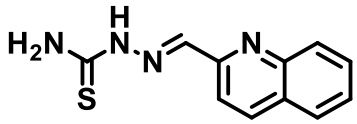

^{1}H NMR (500 MHz, DMSO-d$_6$) δ 11.82 (s, 1H), 8.49 – 8.44 (m, 2H), 8.39 – 8.33 (m, 2H), 8.23 (s, 1H), 8.00 (dd, *J* = 14.1, 9.1 Hz, 2H), 7.81 – 7.74 (m, 1H), 7.62 (t, *J* = 7.5 Hz, 1H).

M$_1$

^{1}H NMR (500 MHz, DMSO-d$_6$) δ 11.81 (s, 1H), 8.45 (t, *J* = 7.0 Hz, 2H), 8.37 (d, *J* = 8.7 Hz, 2H), 8.23 (s, 1H), 8.04 – 7.92 (m, 3H), 7.77 (d, *J* = 8.2 Hz, 1H), 7.62 (t, *J* = 7.8 Hz, 1H).

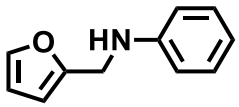

(3a)^{1}H NMR (400 MHz, CDCl$_3$) δ 7.40 (s, 1H), 7.23 (t, *J* = 8.0 Hz, 2H), 6.78 (t, *J* = 7.3 Hz, 1H), 6.71 (d, *J* = 7.5 Hz, 2H), 6.36 (s, 1H), 6.27 (s, 1H), 4.34 (s, 2H), 4.04 (s, 1H).

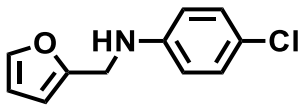

(3b) ^{1}H NMR (400 MHz, CDCl$_3$) δ 7.36 (s, 1H), 7.13 (d, *J* = 8.9 Hz, 2H), 6.59 (d, *J* = 8.9 Hz, 2H), 6.33 (d, *J* = 3.3 Hz, 1H), 6.23 (d, *J* = 3.4 Hz, 1H), 4.29 (s, 2H), 4.05 (s, 1H).

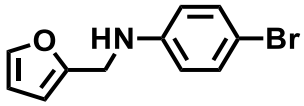

(3c) ^{1}H NMR (400 MHz, $CDCl_3$) δ 7.40 (s, 1H), 7.29 (d, *J* = 8.9 Hz, 2H), 6.57 (d, *J* = 8.9 Hz, 2H), 6.35 (d, *J* = 3.3 Hz, 1H), 6.25 (d, *J* = 3.3 Hz, 1H), 4.31 (s, 2H), 4.08 (s, 1H).

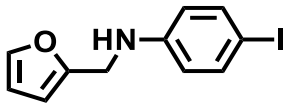

(3d) ^{1}H NMR (400 MHz, $CDCl_3$) δ 7.43 (d, *J* = 8.9 Hz, 2H), 7.37 (s, 1H), 6.45 (d, *J* = 8.9 Hz, 2H), 6.38 – 6.28 (m, 1H), 6.23 (d, *J* = 3.5 Hz, 1H), 4.28 (s, 2H), 4.08 (s, H).

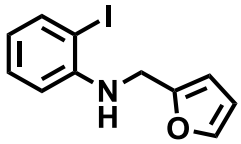

(3e) ^{1}H NMR (400 MHz, $CDCl_3$) δ 7.71 – 7.62 (m, 1H), 7.39 (s, 1H), 7.20 (t, *J* = 8.5 Hz, 1H), 6.65 (d, *J* = 8.1 Hz, 1H), 6.53 – 6.43 (m, 1H), 6.37 – 6.29 (m, 1H), 6.25 (d, *J* = 3.4 Hz, 1H), 4.55 (s, 1H), 4.38 (s, 2H).

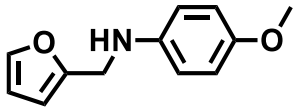

(3f)^{1}H NMR (400 MHz, $CDCl_3$) δ 7.38 (s, 1H), 6.80 (d, *J* = 9.0 Hz, 2H), 6.66 (d, *J* = 8.9 Hz, 2H), 6.36 – 6.31 (m, 1H), 6.23 (d, *J* = 3.6 Hz, 1H), 4.28 (s, 2H), 3.76 (s, 4H).

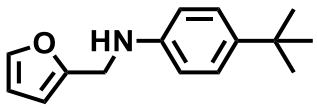

(3g)^{1}H NMR (400 MHz, $CDCl_3$) δ 7.40 (s, 1H), 7.26 (d, *J* = 8.8 Hz, 2H), 6.68 (d, *J* = 8.6 Hz, 2H), 6.39 – 6.32 (m, 1H), 6.27 (d, *J* = 3.4 Hz, 1H), 4.34 (s, 2H), 3.96 (s, 1H) 1.32(s, 9H)

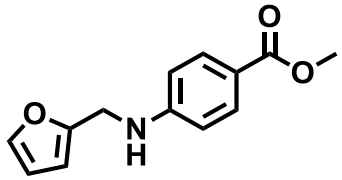

(3h)^{1}H NMR (400 MHz, $CDCl_3$) δ 7.87 (d, *J* = 8.9 Hz, 2H), 7.38 (s, 1H), 6.63 (d, *J* = 8.9 Hz, 2H), 6.38 – 6.31 (m, 1H), 6.25 (d, *J* = 3.4 Hz, 1H), 4.37 (s, 2H), 3.85 (s, 3H).

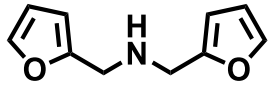

(3i)^{1}H NMR (400 MHz, $CDCl_3$) δ 7.36 (s, 2H), 6.35 – 6.28 (m, 2H), 6.18 (d, *J* = 3.3 Hz, 2H), 3.78 (s, 4H).

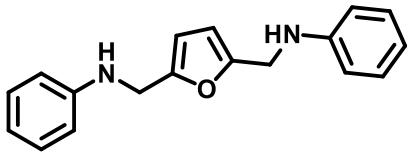

(3j)^{1}H NMR (400 MHz, $CDCl_3$) δ 7.20 (t, *J* = 7.8 Hz, 4H), 6.76 (t, *J* = 7.3 Hz, 2H), 6.69 (s, 4H), 6.17 (s, 2H), 4.29 (s, 4H), 4.01 (s, 2H).

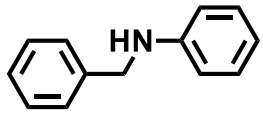

(3k)^{1}H NMR (400 MHz, $CDCl_3$) δ 7.42 – 7.27 (m, 5H), 7.19 (t, *J* = 8.0 Hz, 2H), 6.73 (t, *J* = 7.3 Hz, 1H), 6.66 (d, *J* = 7.8 Hz, 2H), 4.35 (s, 2H), 4.04 (s, 1H).

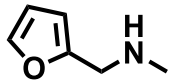

(3m)^{1}H NMR (400 MHz, $CDCl_3$) δ 7.35 (s, 1H), 6.37 – 6.27 (m, 1H), 6.17 (d, *J* = 3.3 Hz, 1H), 3.73 (s, 2H), 2.42 (s, 3H).

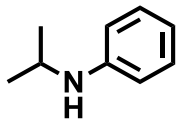

(3n)^{1}H NMR (400 MHz, $CDCl_3$) δ 7.23 – 7.07 (m, 2H), 6.68 (t, *J* = 7.4 Hz, 1H), 6.59 (d, *J* = 7.9 Hz, 2H), 3.64 (p, *J* = 6.3 Hz, 1H), 3.45 (s, 1H), 1.22 (d, *J* = 6.4 Hz, 6H).

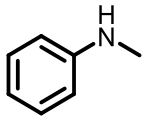

^{1}H NMR (400 MHz, $CDCl_3$) δ 7.21 (t, *J* = 7.8 Hz, 2H), 6.73 (t, *J* = 7.3 Hz, 1H), 6.63 (d, *J* = 8.3 Hz, 2H), 3.70 (s, 1H), 2.85 (s, 3H).

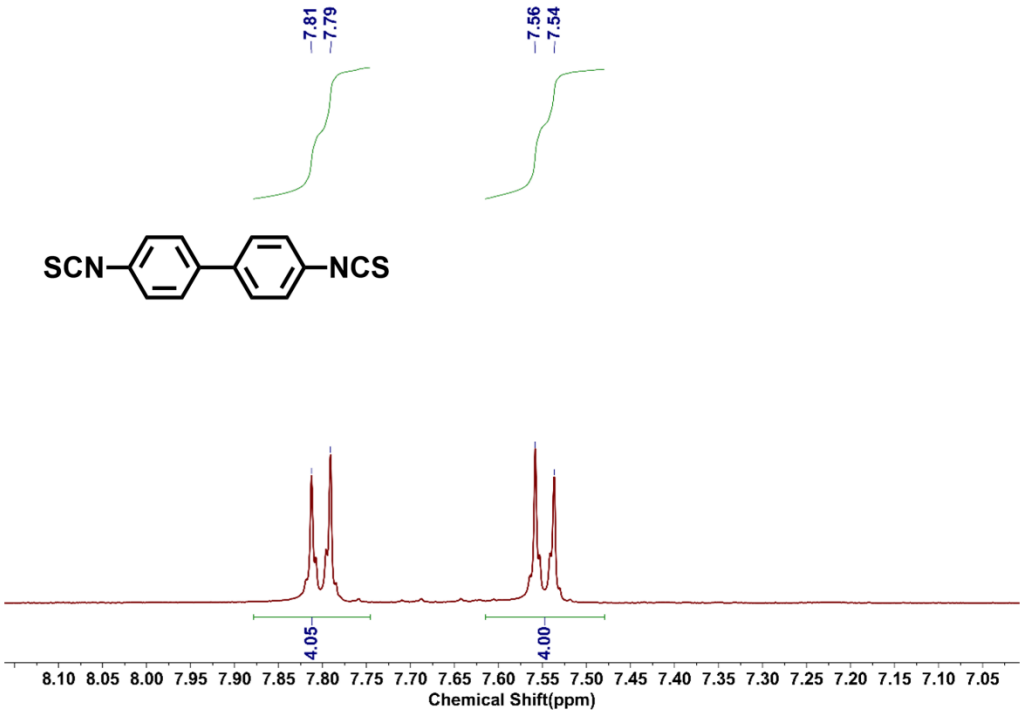
7.81
7.79
7.56
7.54
SCN
NCS
4.05
4.00
8.10 8.05 8.00 7.95 7.90 7.85 7.80 7.75 7.70 7.65 7.60 7.55 7.50 7.45 7.40 7.35 7.30 7.25 7.20 7.15 7.10 7.05
Chemical Shift(ppm)

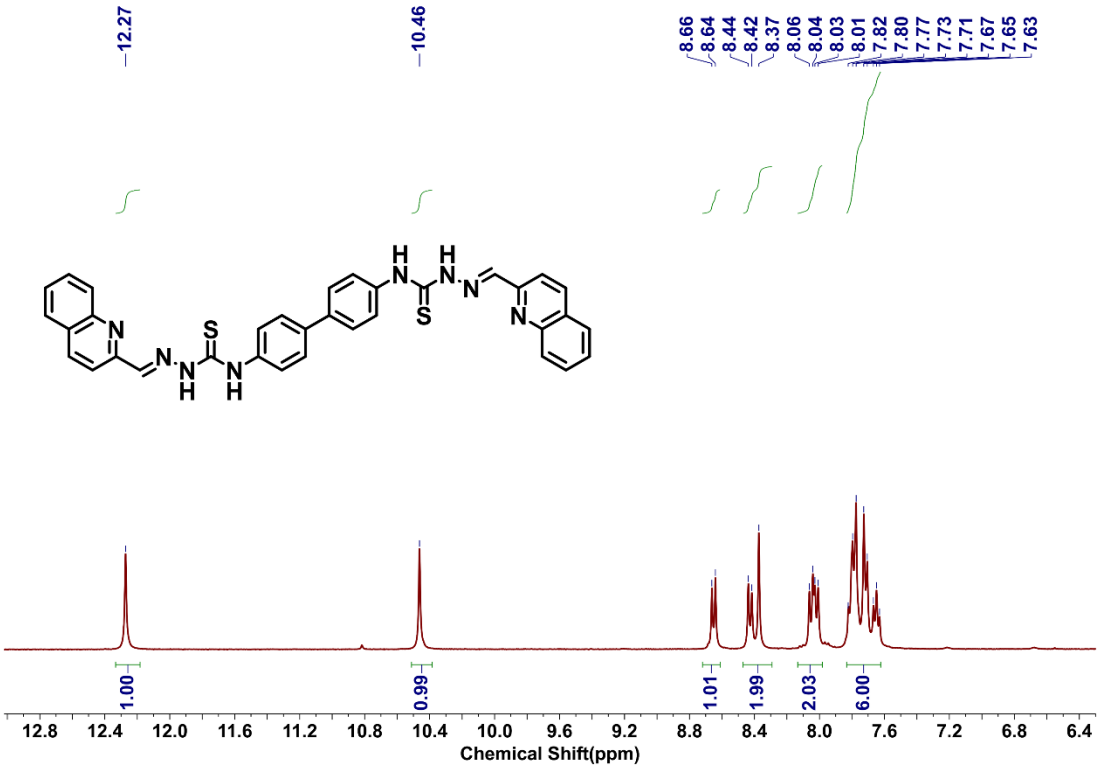
12.27
10.46
8.66
8.64
8.44
8.42
8.37
8.06
8.04
8.03
8.01
7.82
7.80
7.77
7.73
7.71
7.67
7.65
7.63
1.00
0.99
1.01
1.99
2.03
6.00
12.8 12.4 12.0 11.6 11.2 10.8 10.4 10.0 9.6 9.2 8.8 8.4 8.0 7.6 7.2 6.8 6.4
Chemical Shift(ppm)

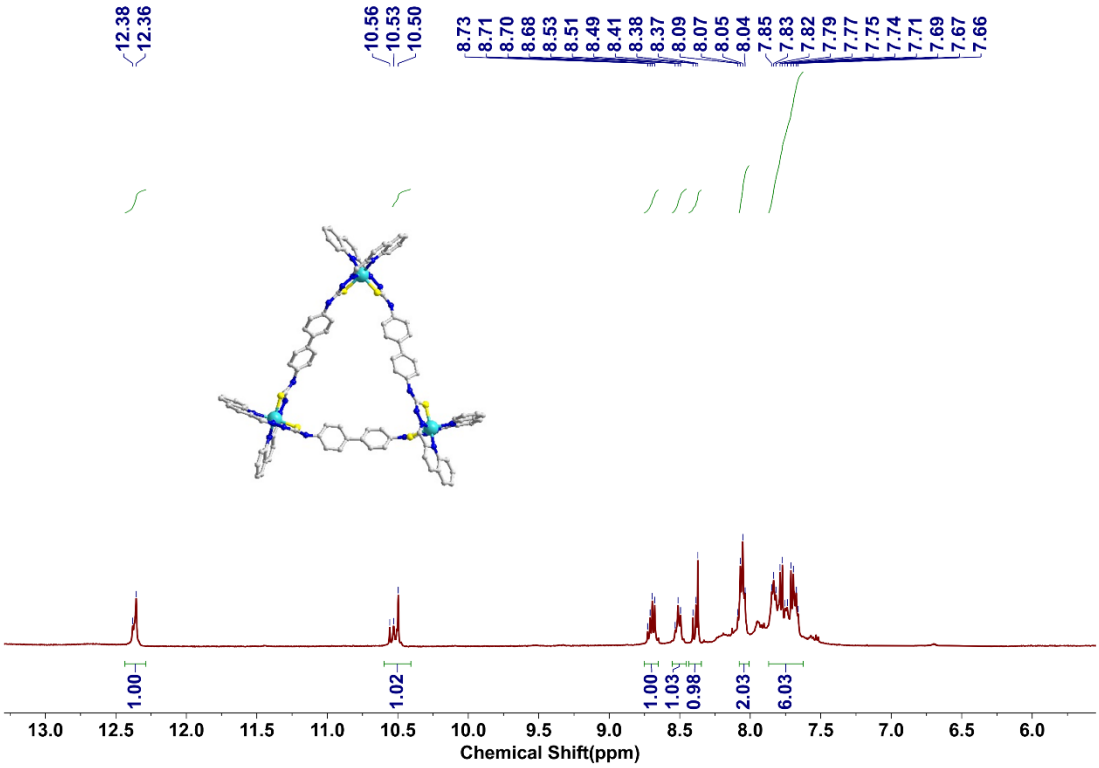
12.38
12.36
10.56
10.53
10.50
8.73
8.71
8.70
8.68
8.53
8.51
8.49
8.41
8.38
8.37
8.09
8.07
8.05
8.04
7.85
7.83
7.82
7.79
7.77
7.75
7.74
7.71
7.69
7.67
7.66
1.00
1.02
1.00
1.03
0.98
2.03
6.03
13.0
12.5
12.0
11.5
11.0
10.5
10.0
9.5
9.0
8.5
8.0
7.5
7.0
6.5
6.0
Chemical Shift(ppm)

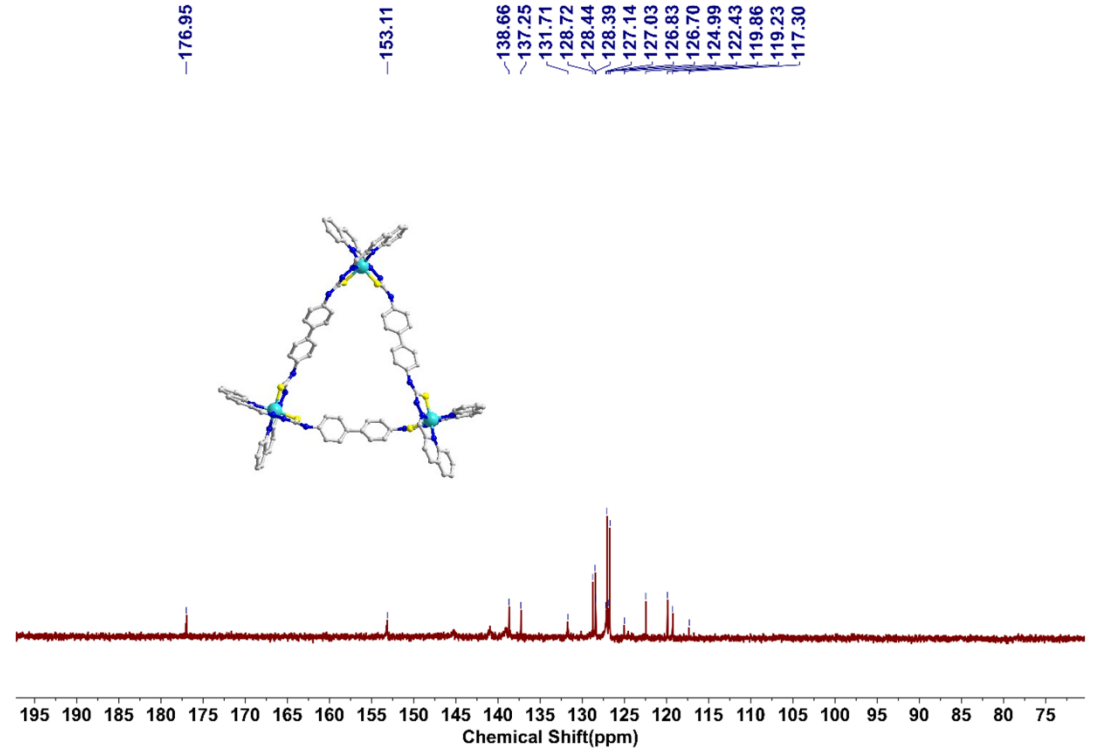
176.95
153.11
138.66
137.25
131.71
128.72
128.44
128.39
127.14
127.03
126.83
126.70
124.99
122.43
119.86
119.23
117.30
195
190
185
180
175
170
165
160
155
150
145
140
135
130
125
120
115
110
105
100
95
90
85
80
75
Chemical Shift(ppm)

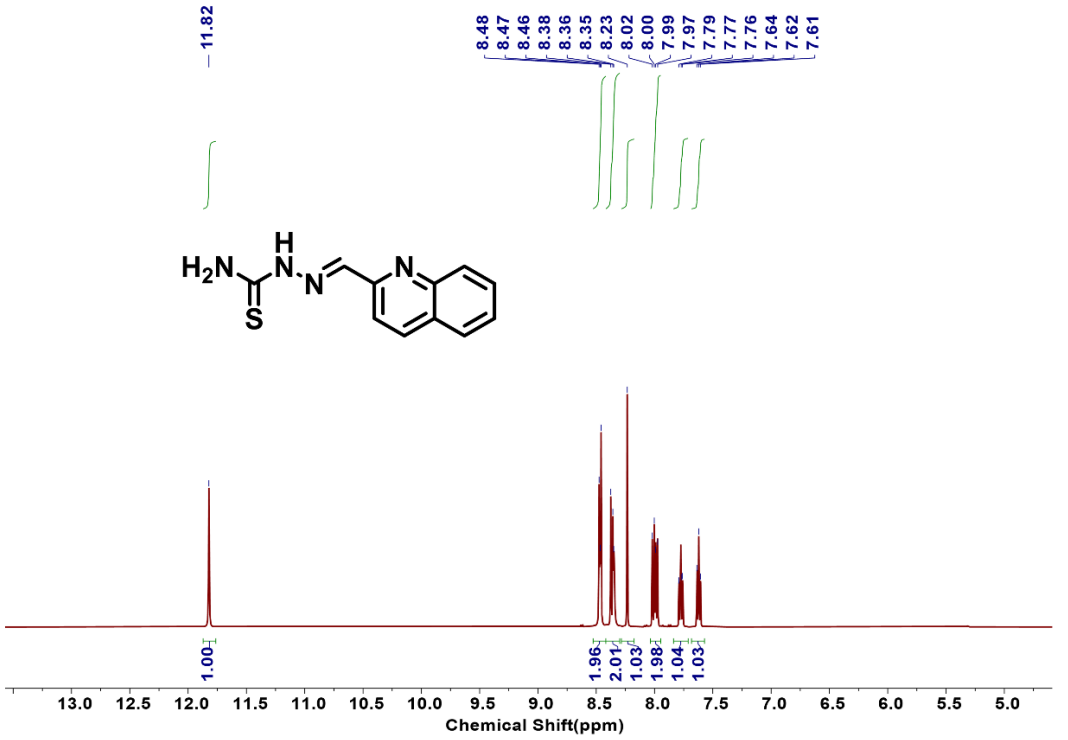
11.82
8.48
8.47
8.46
8.38
8.36
8.35
8.23
8.02
8.00
7.99
7.97
7.79
7.77
7.76
7.64
7.62
7.61
H2N
H
N
N
S
1.00
1.96
2.01
1.03
1.98
1.04
1.03
13.0
12.5
12.0
11.5
11.0
10.5
10.0
9.5
9.0
8.5
8.0
7.5
7.0
6.5
6.0
5.5
5.0
Chemical Shift(ppm)

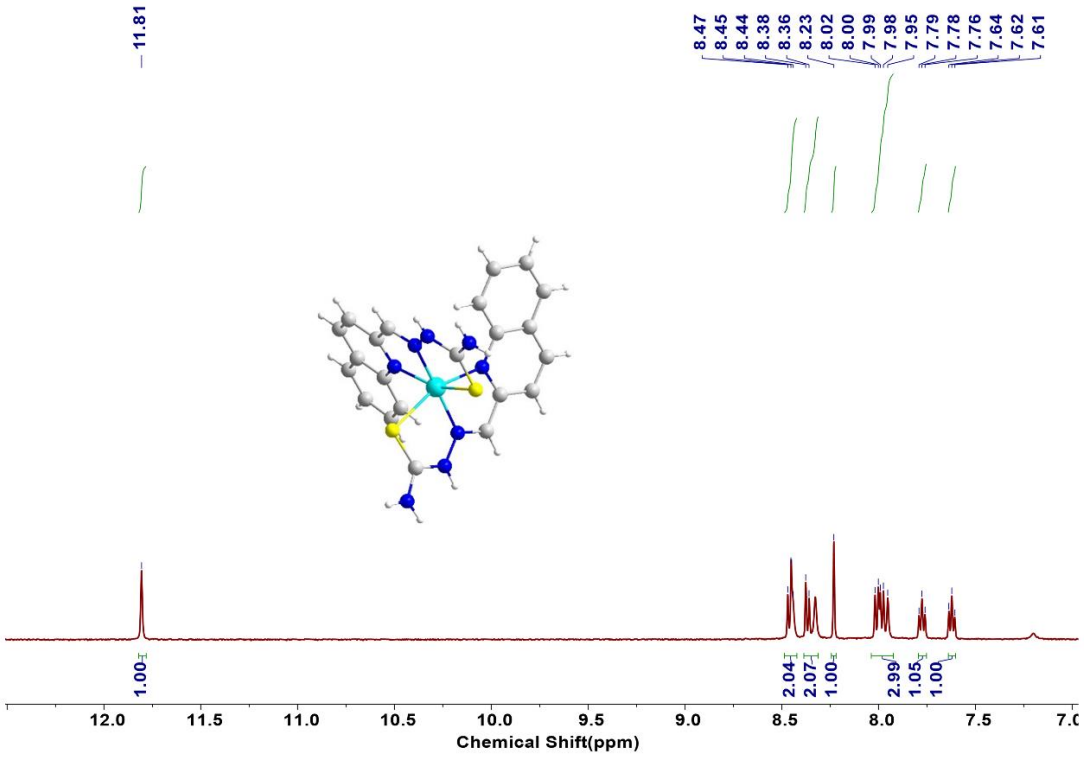
11.81
8.47
8.45
8.44
8.38
8.36
8.23
8.02
8.00
7.99
7.98
7.95
7.79
7.78
7.76
7.64
7.62
7.61
1.00
2.04
2.07
1.00
2.99
1.05
1.00
12.0
11.5
11.0
10.5
10.0
9.5
9.0
8.5
8.0
7.5
7.0
Chemical Shift(ppm)

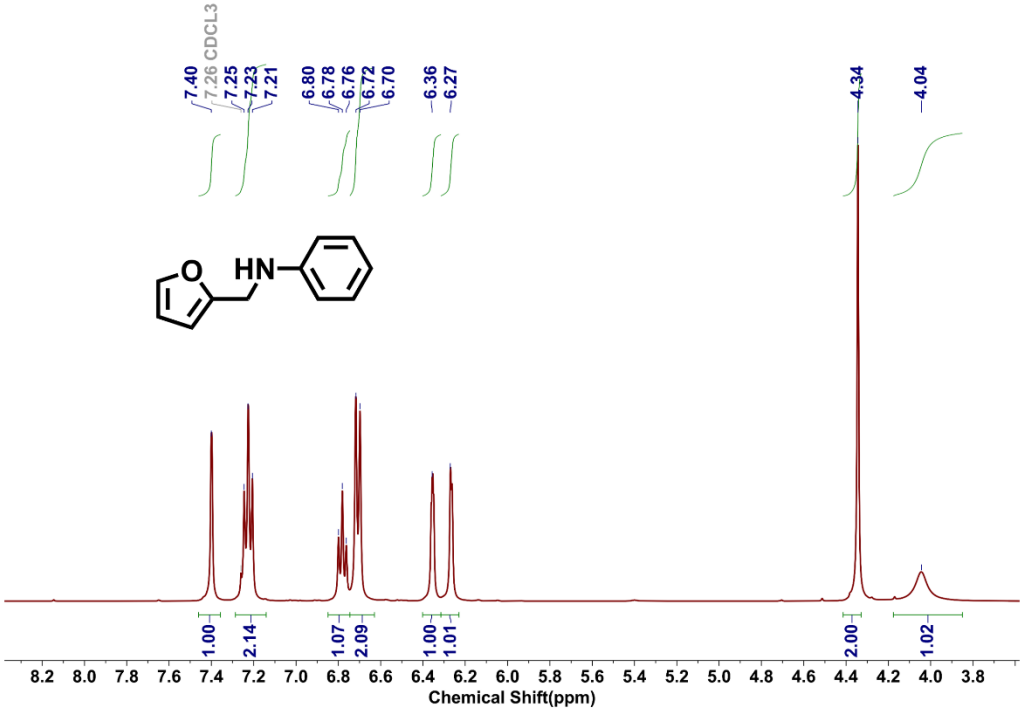
7.40
7.26 CDCL3
7.25
7.23
7.21
6.80
6.78
6.76
6.72
6.70
6.36
6.27
4.34
4.04
O
HN
1.00
2.14
1.07
2.09
1.00
1.01
2.00
1.02
8.2 8.0 7.8 7.6 7.4 7.2 7.0 6.8 6.6 6.4 6.2 6.0 5.8 5.6 5.4 5.2 5.0 4.8 4.6 4.4 4.2 4.0 3.8
Chemical Shift(ppm)

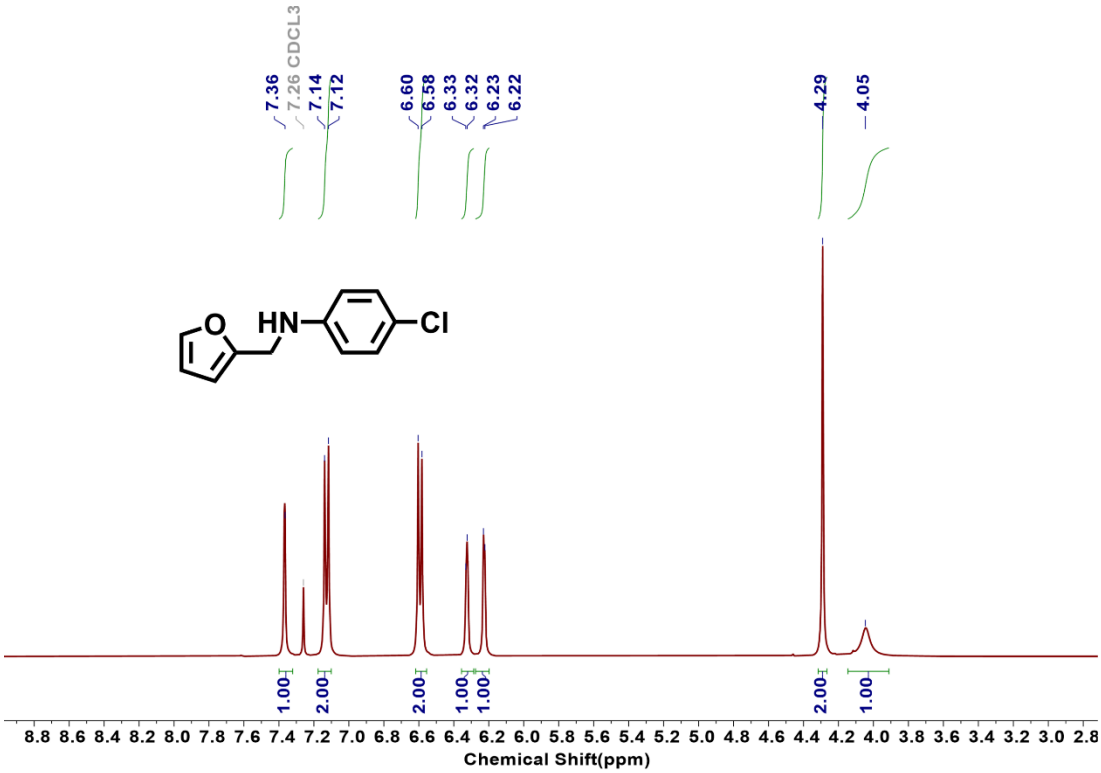
7.36
7.26 CDCL3
7.14
7.12
6.60
6.58
6.33
6.32
6.23
6.22
4.29
4.05
O
HN
Cl
1.00
2.00
2.00
1.00
1.00
2.00
1.00
8.8 8.6 8.4 8.2 8.0 7.8 7.6 7.4 7.2 7.0 6.8 6.6 6.4 6.2 6.0 5.8 5.6 5.4 5.2 5.0 4.8 4.6 4.4 4.2 4.0 3.8 3.6 3.4 3.2 3.0 2.8
Chemical Shift(ppm)

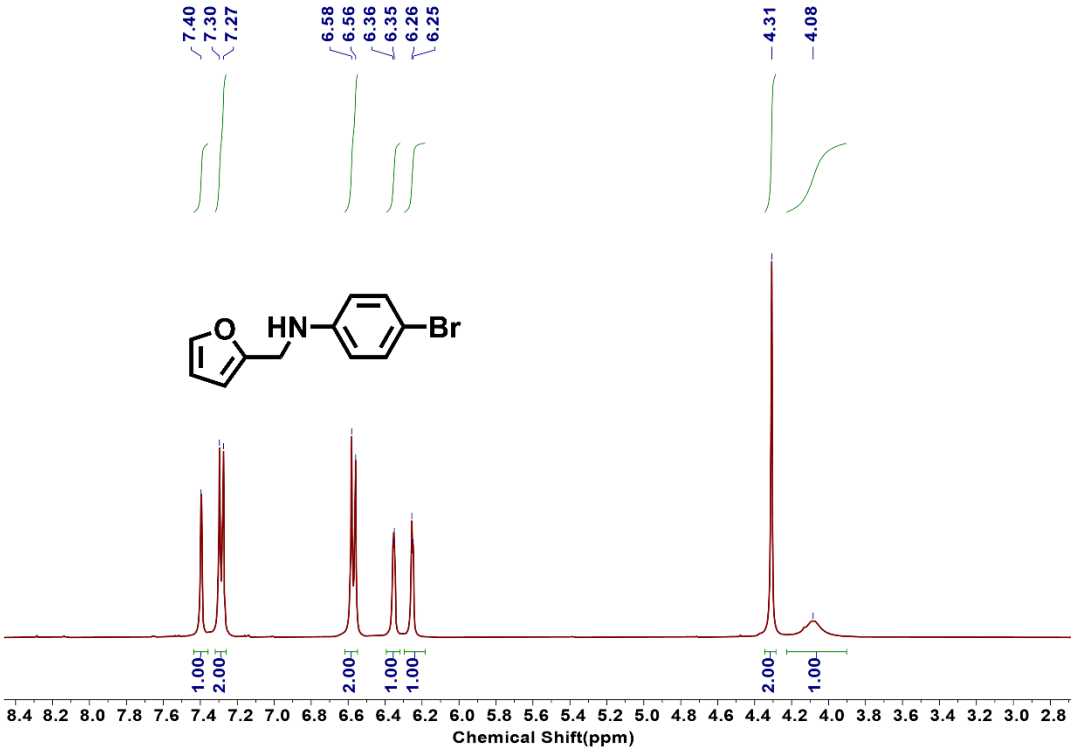
7.40
7.30
7.27
6.58
6.56
6.36
6.35
6.26
6.25
4.31
4.08
O
HN
Br
1.00
2.00
2.00
1.00
1.00
2.00
1.00
8.4 8.2 8.0 7.8 7.6 7.4 7.2 7.0 6.8 6.6 6.4 6.2 6.0 5.8 5.6 5.4 5.2 5.0 4.8 4.6 4.4 4.2 4.0 3.8 3.6 3.4 3.2 3.0 2.8
Chemical Shift(ppm)

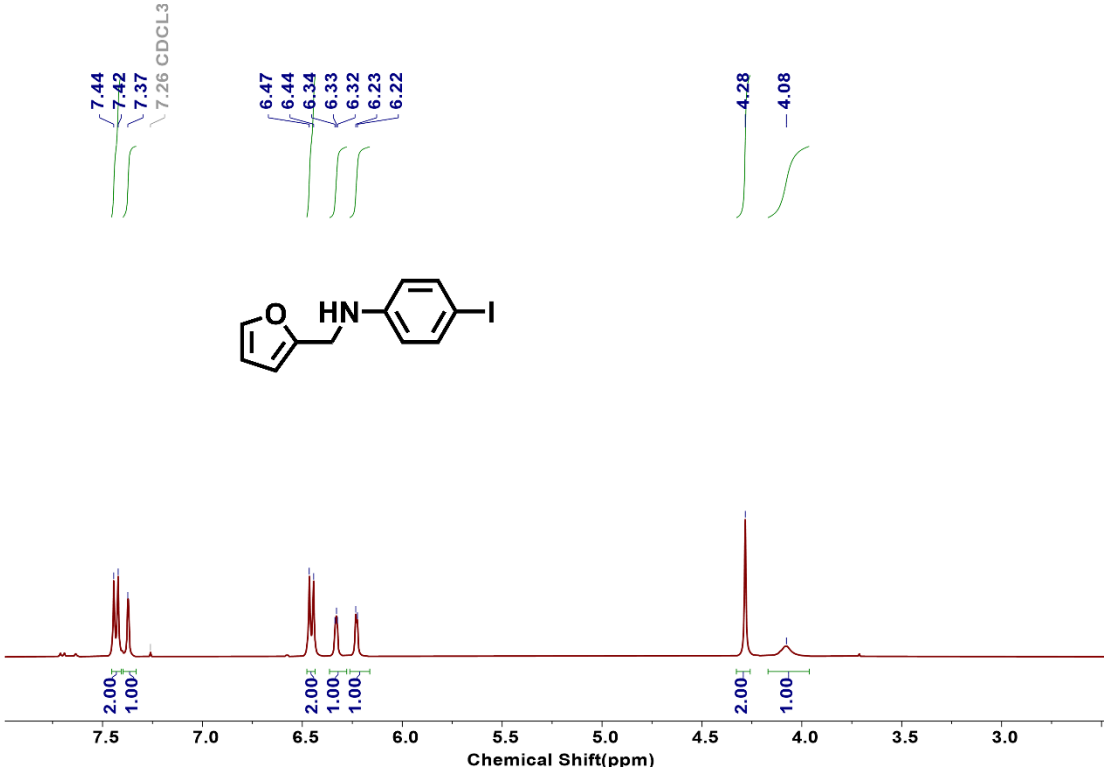
7.44
7.42
7.37
7.26 CDCL3
6.47
6.44
6.34
6.33
6.32
6.23
6.22
4.28
4.08
O
HN
I
2.00
1.00
2.00
1.00
1.00
2.00
1.00
7.5 7.0 6.5 6.0 5.5 5.0 4.5 4.0 3.5 3.0
Chemical Shift(ppm)

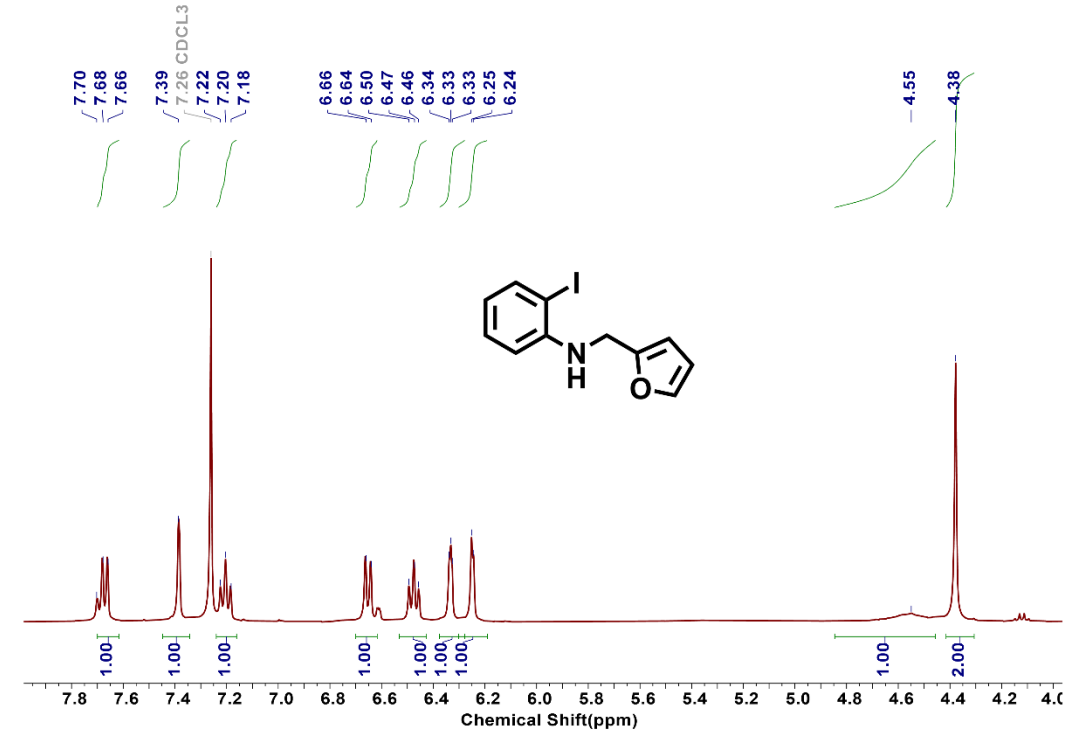
7.70
7.68
7.66
7.39
7.26 CDCL3
7.22
7.20
7.18
6.66
6.64
6.50
6.47
6.46
6.34
6.33
6.33
6.25
6.24
4.55
4.38
I
N
H
O
1.00
1.00
1.00
1.00
1.00
1.00
1.00
1.00
2.00
7.8 7.6 7.4 7.2 7.0 6.8 6.6 6.4 6.2 6.0 5.8 5.6 5.4 5.2 5.0 4.8 4.6 4.4 4.2 4.0
Chemical Shift(ppm)

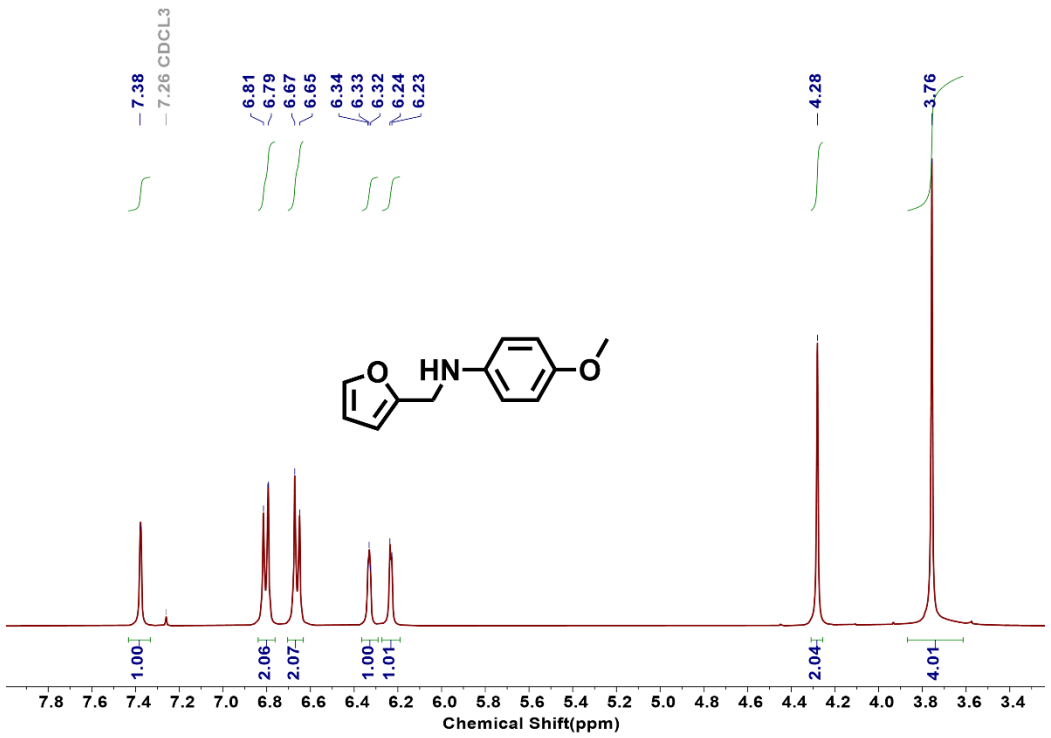
7.38
7.26 CDCL3
6.81
6.79
6.67
6.65
6.34
6.33
6.32
6.24
6.23
4.28
3.76
O
HN
O
1.00
2.06
2.07
1.00
1.01
2.04
4.01
7.8 7.6 7.4 7.2 7.0 6.8 6.6 6.4 6.2 6.0 5.8 5.6 5.4 5.2 5.0 4.8 4.6 4.4 4.2 4.0 3.8 3.6 3.4
Chemical Shift(ppm)

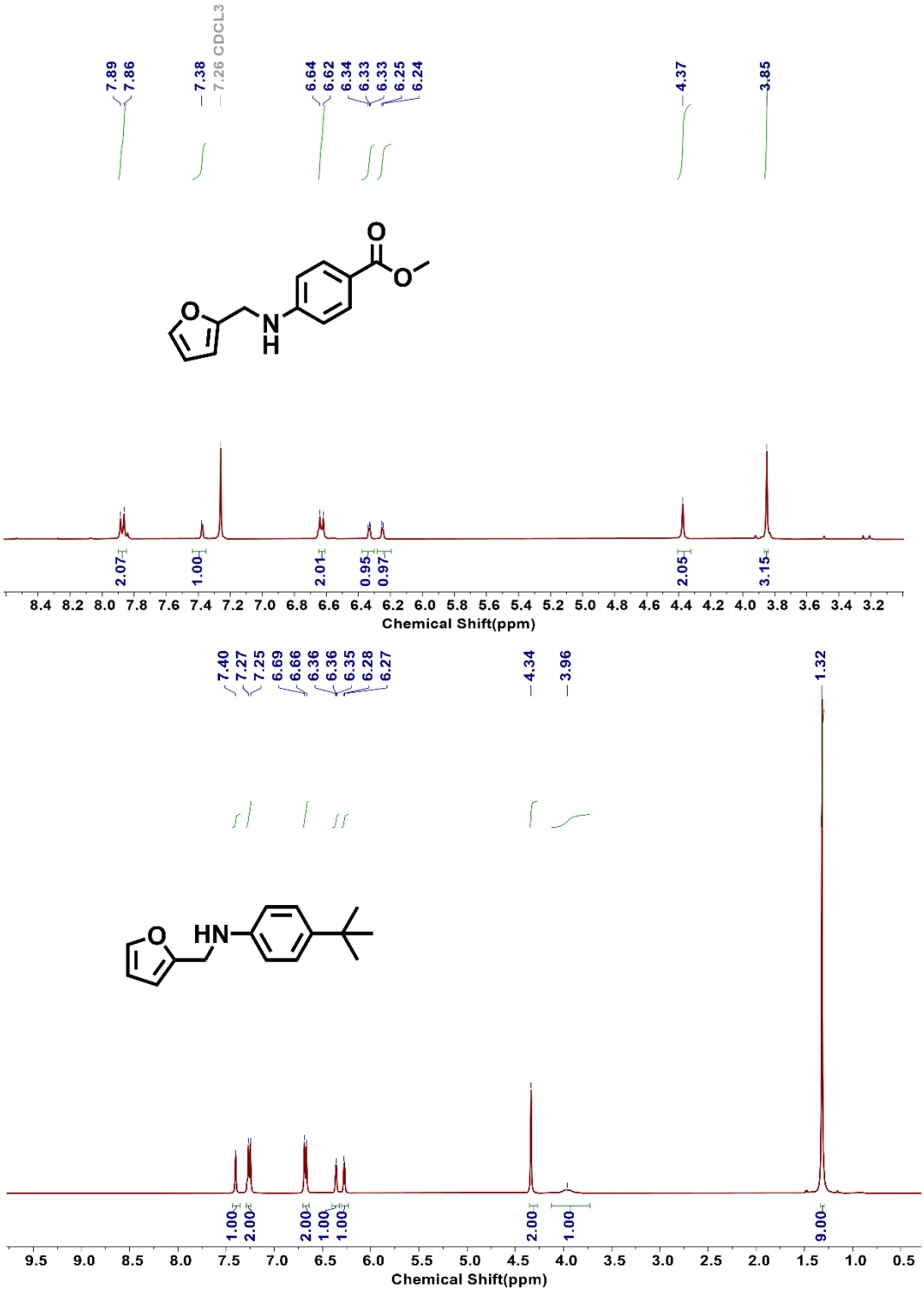
7.89
7.86
7.38
7.26 CDCL3
6.64
6.62
6.34
6.33
6.33
6.25
6.24
4.37
3.85
O
O
O
N
H
2.07
1.00
2.01
0.95
0.97
2.05
3.15
8.4 8.2 8.0 7.8 7.6 7.4 7.2 7.0 6.8 6.6 6.4 6.2 6.0 5.8 5.6 5.4 5.2 5.0 4.8 4.6 4.2 4.0 3.8 3.6 3.4 3.2
Chemical Shift(ppm)
7.40
7.27
7.25
6.69
6.66
6.36
6.36
6.35
6.28
6.27
4.34
3.96
1.32
O
HN
1.00
2.00
2.00
1.00
1.00
2.00
1.00
9.00
9.5 9.0 8.5 8.0 7.5 7.0 6.5 6.0 5.5 5.0 4.5 4.0 3.5 3.0 2.5 2.0 1.5 1.0 0.5
Chemical Shift(ppm)

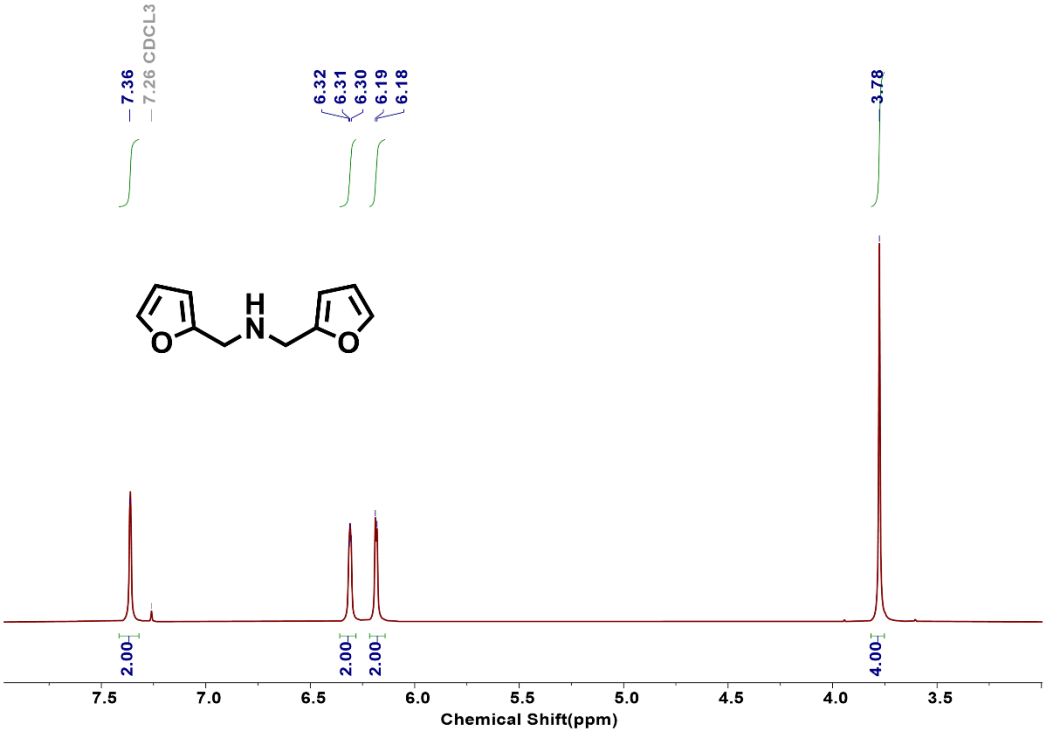
7.36
7.26 CDCL3
6.32
6.31
6.30
6.19
6.18
3.78
2.00
2.00
2.00
4.00
7.5
7.0
6.5
6.0
5.5
5.0
4.5
4.0
3.5
Chemical Shift(ppm)

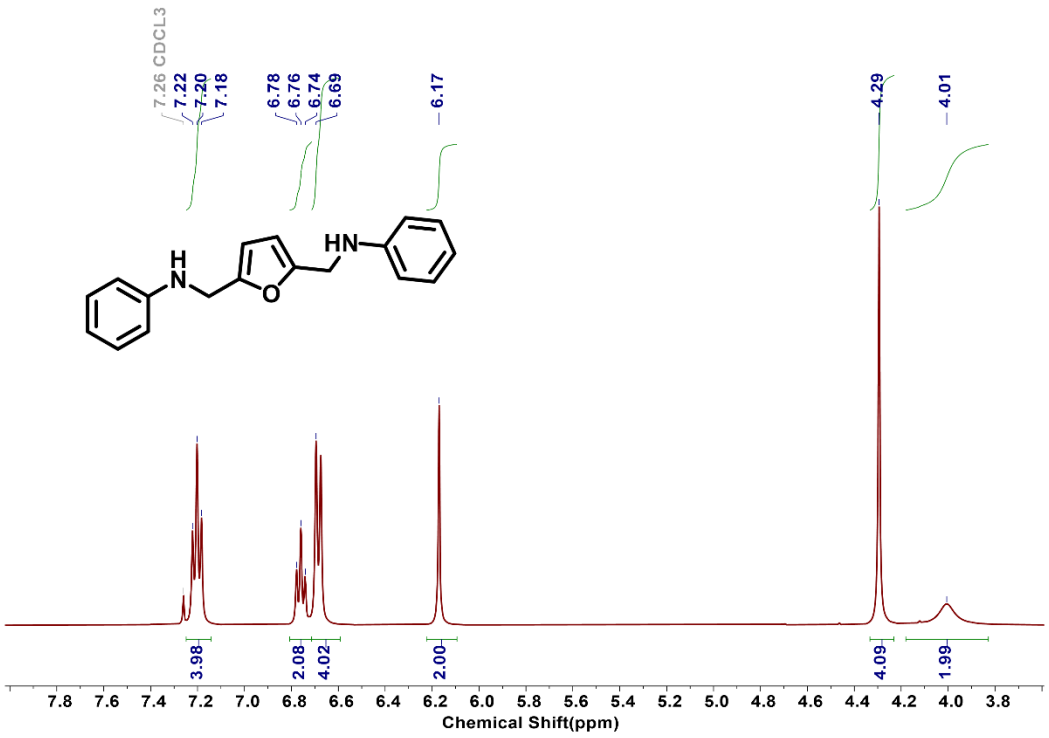
7.26 CDCL3
7.22
7.20
7.18
6.78
6.76
6.74
6.69
6.17
4.29
4.01
3.98
2.08
4.02
2.00
4.09
1.99
7.8
7.6
7.4
7.2
7.0
6.8
6.6
6.4
6.2
6.0
5.8
5.6
5.4
5.2
5.0
4.8
4.6
4.4
4.2
4.0
3.8
Chemical Shift(ppm)

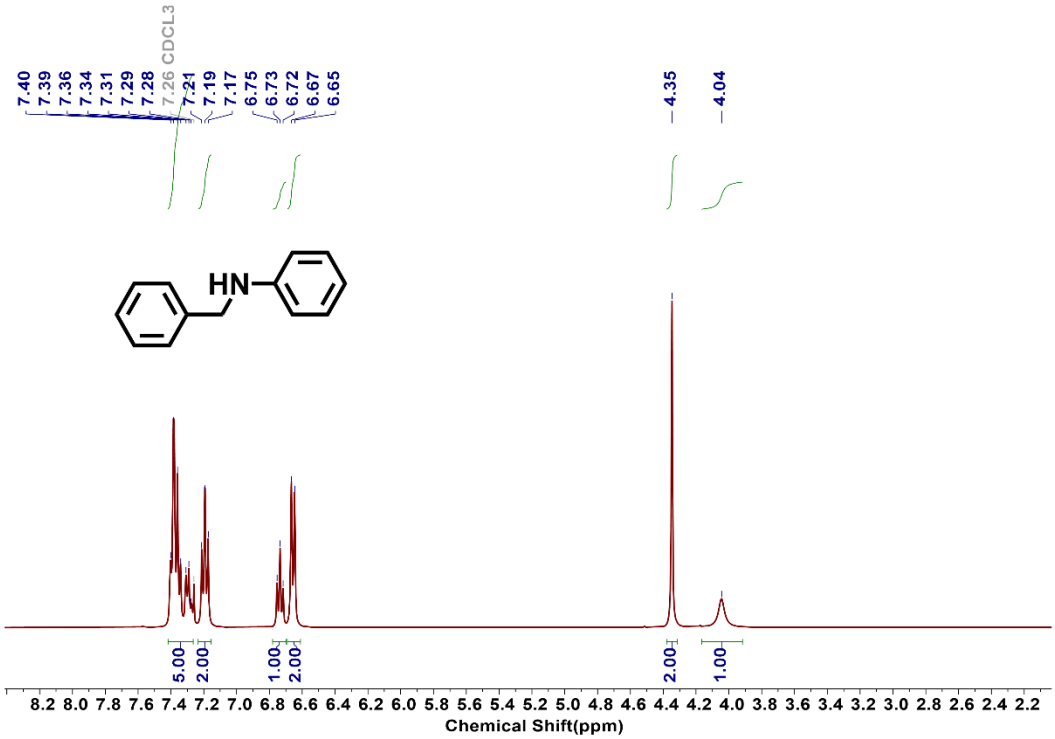
7.40
7.39
7.36
7.34
7.31
7.29
7.28
7.26 CDCL3
7.21
7.19
7.17
6.75
6.73
6.72
6.67
6.65
4.35
4.04
HN
5.00
2.00
1.00
2.00
2.00
1.00
8.2 8.0 7.8 7.6 7.4 7.2 7.0 6.8 6.6 6.4 6.2 6.0 5.8 5.6 5.4 5.2 5.0 4.8 4.6 4.4 4.2 4.0 3.8 3.6 3.4 3.2 3.0 2.8 2.6 2.4 2.2
Chemical Shift(ppm)

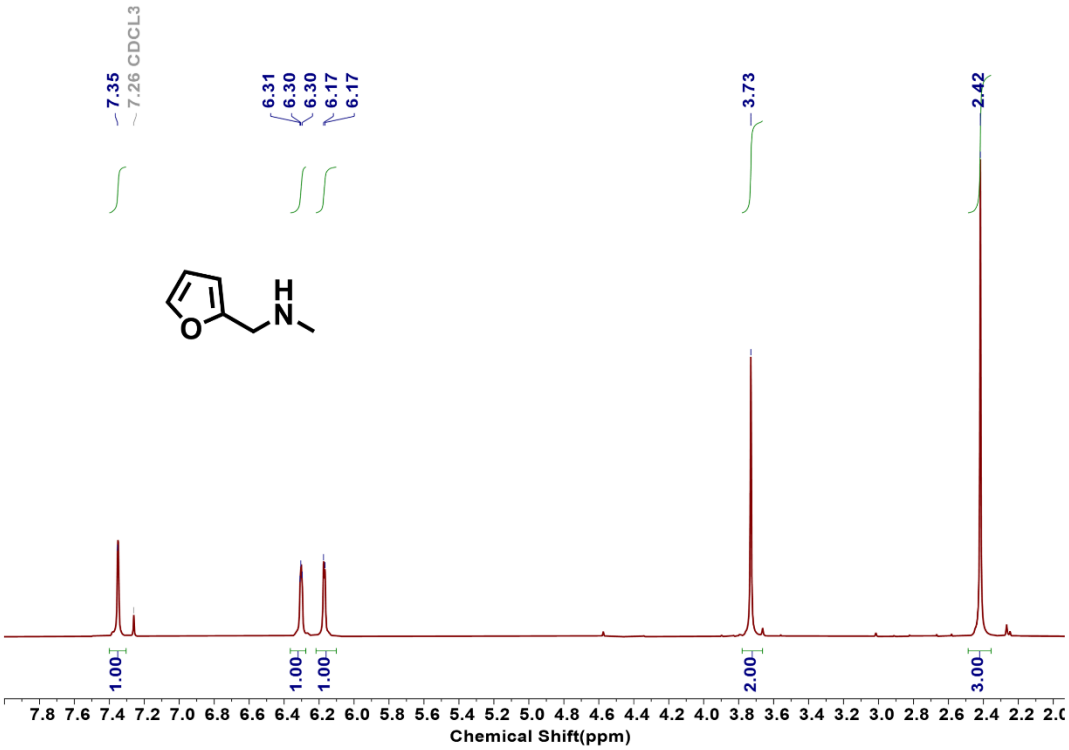
7.35
7.26 CDCL3
6.31
6.30
6.30
6.17
6.17
3.73
2.42
O
H
N
1.00
1.00
1.00
2.00
3.00
7.8 7.6 7.4 7.2 7.0 6.8 6.6 6.4 6.2 6.0 5.8 5.6 5.4 5.2 5.0 4.8 4.6 4.4 4.2 4.0 3.8 3.6 3.4 3.2 3.0 2.8 2.6 2.4 2.2 2.0
Chemical Shift(ppm)

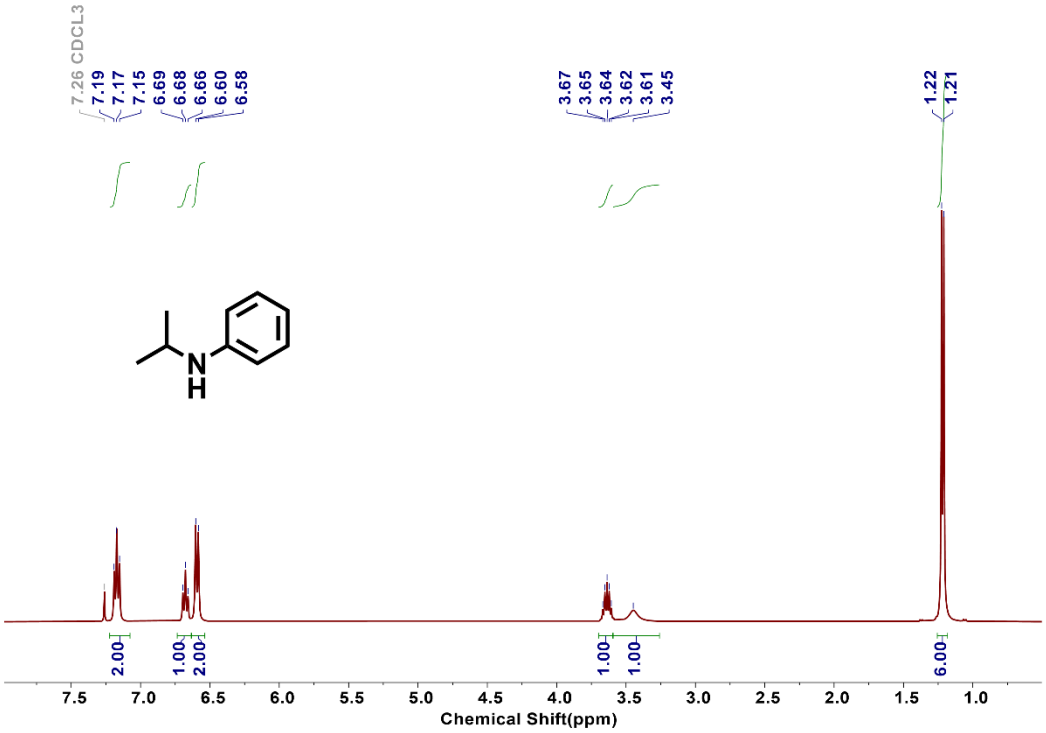
7.26 CDCL3
7.19
7.17
7.15
6.69
6.68
6.66
6.60
6.58
3.67
3.65
3.64
3.62
3.61
3.45
1.22
1.21
2.00
1.00
2.00
1.00
1.00
6.00
7.5
7.0
6.5
6.0
5.5
5.0
4.5
4.0
3.5
3.0
2.5
2.0
1.5
1.0
Chemical Shift(ppm)

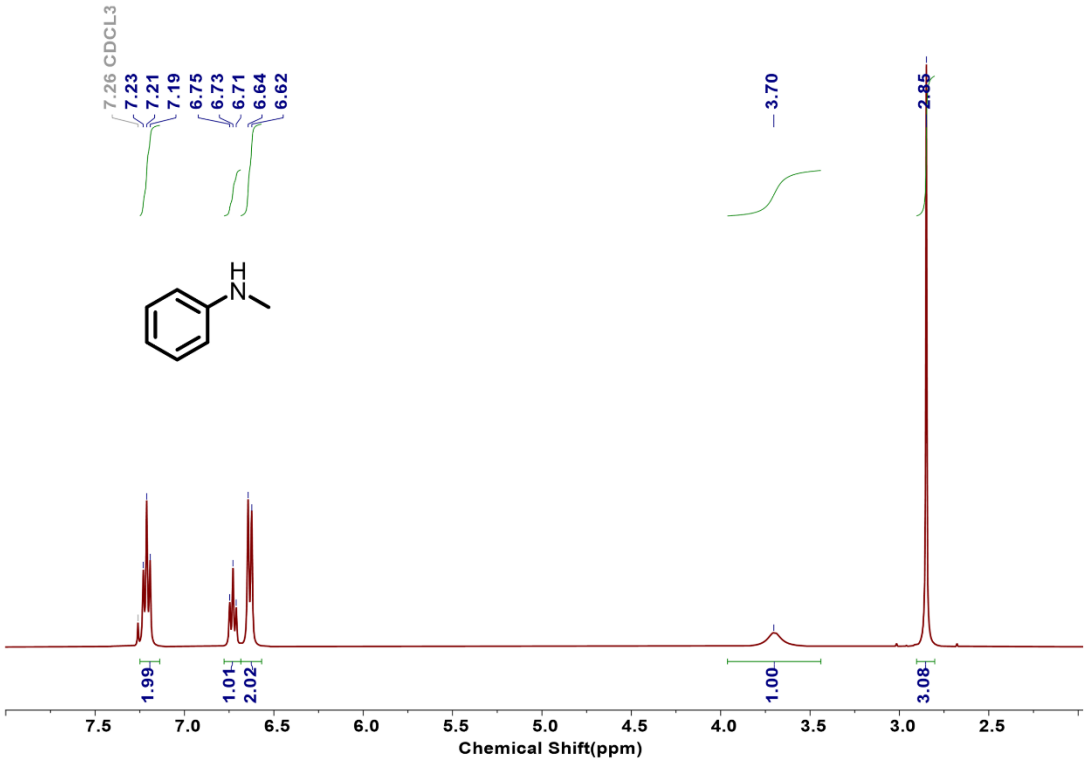
7.26 CDCL3
7.23
7.21
7.19
6.75
6.73
6.71
6.64
6.62
3.70
2.85
1.99
1.01
2.02
1.00
3.08
7.5
7.0
6.5
6.0
5.5
5.0
4.5
4.0
3.5
3.0
2.5
Chemical Shift(ppm)

References

1. G. M. Sheldrick, SADABS. Software for empirical absorption corrections, University of Göttingen, Germany, 2000.
2. G. Sheldrick, *Acta Crystallogr. Sect.* A. 2008, **64**, 112-122.
3. A. L. Spek, J. *Appl. Crystallogr.* 2003, **36**, 7-13.
4. Y. Yang, X. Jing, Y. Shi, Y. Wu and C. Duan, *J. Am. Chem. Soc.*, 2023, **145**, 10136–10148.
5. J. Wei, L. Zhao, Y. Zhang, G. Han, C. He, C. Wang and C. Duan, *J. Am. Chem. Soc.*, 2023, **145**, 6719–6729.
6. A. Macchioni, G. Ciancaleoni, C. Zuccaccia and D. Zuccaccia, *Chem Soc Rev*, 2008, **37**, 479–489
7. L. Avram and Y. Cohen, *Chem. Soc. Rev.*, 2015, **44**, 586–602.
8. H. C. Chen and S. H. Chen, *J. Phys. Chem.*, 1984, **88**, 5118–5121
9. F. Perrin *J. Phys. Radium.*, 1936, **7**, 1
10. R. Evans, G. Dal Poggetto, M. Nilsson and G. A. Morris, *Anal. Chem*., 2018, **90**, 3987–3994.
11. A. Paul, M. A. Shipman, D. Y. Onabule, S. Sproules and M. D. Symes, *Chem. Sci.*, 2021, **12**, 5082–5090.
12. T. Suwa, E. Sugiyama, I. Shibata and A. Baba, *Synthesis*, 2000, **6**, 789–800.
13. A. Heydari, S. Khaksar, J. Akbari, M. Esfandyari, M. Pourayoubi and M. Tajbakhsh, *Tetrahedron Lett.*, 2007, **48**, 1135–1138.
14. P. D. Pham, P. Bertus and S. Legoupy, *Chem. Commun.*, 2009, **41**, 6207–6209.
15. B. S. Takale, S. Tao, X. Yu, X. Feng, T. Jin, M. Bao and Y. Yamamoto, *Tetrahedron*, 2015, 71, 7154–7158.
16. H. Sharma, M. Bhardwaj, M. Kour and S. Paul, *Mol. Catal.*, 2017, **435**, 58–68.